

# A critical review on surface-modified nano-catalyst application for the photocatalytic degradation of volatile organic compounds

Zhao, Weichen; Adeel, Muhammad; Zhang, Peng; Zhou, Pingfan; Huang, Lili; Zhao, Yongwen; Ahmad, Muhammad Arslan; Shakoor, Noman; Lou, Benzhen; Jiang, Yaqi; Lynch, Iseult; Rui, Yukui

DOI:  
[10.1039/D1EN00955A](https://doi.org/10.1039/D1EN00955A)

License:  
None: All rights reserved

*Document Version*  
Peer reviewed version

*Citation for published version (Harvard):*  
Zhao, W, Adeel, M, Zhang, P, Zhou, P, Huang, L, Zhao, Y, Ahmad, MA, Shakoor, N, Lou, B, Jiang, Y, Lynch, I & Rui, Y 2022, 'A critical review on surface-modified nano-catalyst application for the photocatalytic degradation of volatile organic compounds', *Environmental Science: Nano*, vol. 9, no. 1, pp. 61-80.  
<https://doi.org/10.1039/D1EN00955A>

[Link to publication on Research at Birmingham portal](#)

## General rights

Unless a licence is specified above, all rights (including copyright and moral rights) in this document are retained by the authors and/or the copyright holders. The express permission of the copyright holder must be obtained for any use of this material other than for purposes permitted by law.

- Users may freely distribute the URL that is used to identify this publication.
- Users may download and/or print one copy of the publication from the University of Birmingham research portal for the purpose of private study or non-commercial research.
- User may use extracts from the document in line with the concept of 'fair dealing' under the Copyright, Designs and Patents Act 1988 (?)
- Users may not further distribute the material nor use it for the purposes of commercial gain.

Where a licence is displayed above, please note the terms and conditions of the licence govern your use of this document.

When citing, please reference the published version.

## Take down policy

While the University of Birmingham exercises care and attention in making items available there are rare occasions when an item has been uploaded in error or has been deemed to be commercially or otherwise sensitive.

If you believe that this is the case for this document, please contact [UBIRA@lists.bham.ac.uk](mailto:UBIRA@lists.bham.ac.uk) providing details and we will remove access to the work immediately and investigate.

1 **A critical review on surface modified nano-catalysts**  
2 **application for photocatalytic degradation of volatile organic**  
3 **compounds**

4 Weichen Zhao<sup>a†</sup>, Muhammad Adeel<sup>b†</sup>, Peng Zhang<sup>c,d</sup>, Pingfan Zhou<sup>a</sup>, Lili Huang<sup>f</sup>, Yongwen  
5 Zhao<sup>f</sup>, Muhammad Arslan Ahmad<sup>e</sup>, Noman Shakoor<sup>a</sup>, Benzhen Lou<sup>a</sup>, Yaqi Jiang<sup>a</sup>, Iseult  
6 Lynch<sup>e</sup>, Yukui Rui<sup>a,g,h\*</sup>

7 <sup>a</sup> Beijing Key Laboratory of Farmland Soil Pollution Prevention and Remediation, College of  
8 Resources and Environmental Sciences, China Agricultural University, Beijing 100193, China

9 <sup>b</sup> BNU-HKUST Laboratory of Green Innovation, Advanced Institute of Natural Sciences,  
10 Beijing Normal University at Zhuhai 519087, China

11 <sup>c</sup> School of Geography, Earth and Environmental Sciences, University of Birmingham,  
12 Edgbaston, Birmingham B15 2TT, United Kingdom.

13 <sup>d</sup> Department of Environmental Science and Engineering, University of Science and  
14 Technology of China, Hefei 230026, China

15 <sup>e</sup> Shenzhen Key Laboratory of Marine Bioresource and Eco-environmental science, College of  
16 Life Sciences and Oceanography, Shenzhen University, Shenzhen 518060, China

17 <sup>f</sup>Jiaer Chen Academician Workstation, Jinan Huaxin Automation Engineering Co., Ltd. ,  
18 Xincheng Road, Shanghe County, Jinan, Shandong, China

19 <sup>g</sup> China Agricultural University Professor Workstation of Yuhuangmiao Town, Shanghe  
20 County, Jinan, Shandong, China

21 <sup>h</sup> China Agricultural University Professor Workstation of Sunji Town, Shanghe County,  
22 Shanghe County, Jinan, Shandong, China

23 \*Corresponding author: Yukui Rui: [ruiyukui@163.com](mailto:ruiyukui@163.com)

24 †These authors contributed equally in this work.

25

26

27

28

29

30

31

32

33

34

35

36

37 **Abstract**

38 Surface modification of nano-catalyst got significant attention due its outstanding  
39 photocatalytic performance with minimum secondary pollution. Photocatalytic oxidation (PCO) is  
40 a promising technology for removing volatile organic compounds (VOCs) due to its higher activity  
41 with minimum secondary pollution. In this review, we have selected literature from the Web of  
42 Science database for nearly 10 years, with most of our sources spanning the past 5 years. Current  
43 review study summarizes the recent reports of nano-catalyst surface modification technology,  
44 including overcoming the internal and external limitations of nano-catalyst, and improving the  
45 method of photocatalytic degradation of VOCs. Additionally, we found that surface modification  
46 greatly enhances the catalytic performance of the nano-catalyst, which is beneficial for the  
47 degradation of VOCs. There are some limitations including low catalytic activity and catalyst  
48 stability. So, in future research, new methods of preparing catalysts and improving their overall  
49 catalyst performance should be managed and paid more attention.

50 **Keywords:** Photocatalytic oxidation; Nano-catalyst; Surface modification; Volatile organic  
51 compounds; Surface chemistry;

52

## 53 **1.Introduction**

54 Air quality has received a widespread attention due to its injurious effects on living organism.  
55 Industries, such as petroleum refining <sup>1</sup>, chemical production <sup>2</sup>, synthetic resin <sup>3</sup>, clothing dyeing <sup>4</sup>  
56 <sup>6</sup>, leather processing <sup>7</sup>, pharmaceutical industry <sup>2, 8</sup>, insecticide production <sup>9</sup>, coating and adhesive  
57 manufacturing <sup>10</sup>, spraying <sup>11</sup>, printing <sup>4, 12</sup>, electronic component manufacturing <sup>2, 5, 13</sup> releasing  
58 significant amount of volatile organic compound (VOC) which ultimately effects the air quality (**Fig.**  
59 **1**). Due to easy diffusivity, toxicity and volatility, VOCs can cause irreversible damage to human  
60 health <sup>14-16</sup>. The adverse effects of VOCs on human health include not only acute irritation to the  
61 eyes and lung but also chronic diseases such as asthma, gastrointestinal diseases, cardiovascular  
62 diseases and cancer <sup>17-20</sup>.

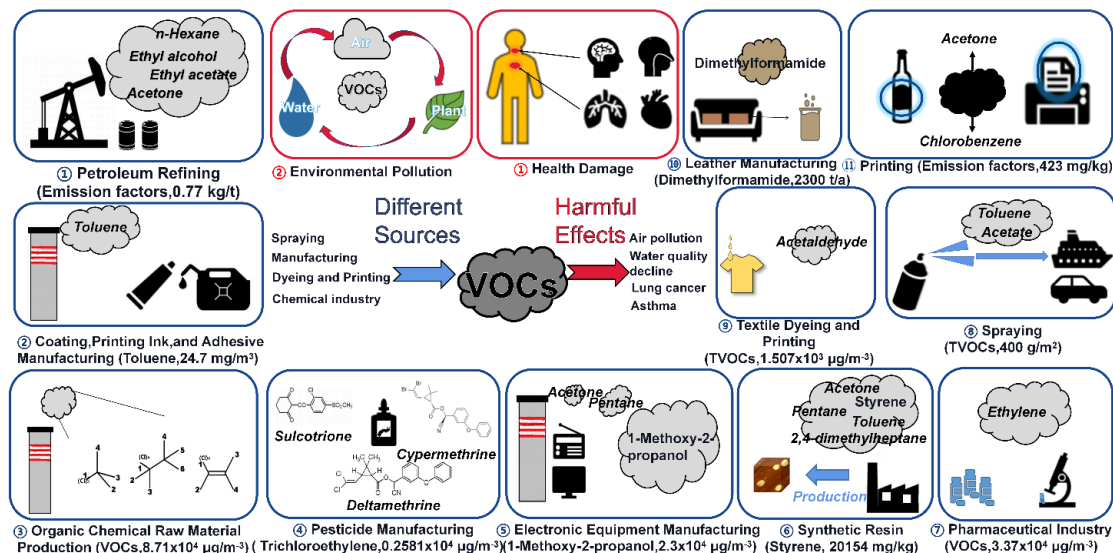
63 To overcome devastating effects of VOCs, several efficient purification techniques of VOCs  
64 has been developed. Such as incineration, condensation, adsorption, photocatalytic oxidation (PCO),  
65 ozone-catalytic oxidation and membrane separation <sup>21</sup>. Comparing with these techniques, PCO has  
66 many advantages such as room-temperature operation, high activity, and no secondary pollution  
67 which made PCO an auspicious technique<sup>22</sup>. Besides, PCO is a powerful air purification technology  
68 that destroys VOCs, by photocatalysis under the irradiation of ultraviolet (UV) and sunlight,  
69 converting them to water, carbon dioxide and detritus.

70 Commonly used photocatalysts material for purification of VOCs includes TiO<sub>2</sub>, ZnO, WO<sub>3</sub>,  
71 V<sub>2</sub>O<sub>5</sub>, ZnS and CdS <sup>23-25</sup>. To date, nanotechnology has made exponential progress <sup>26-28</sup>.  
72 Nanomaterials (NMs) are widely used in the field of environmental remediation <sup>29</sup>. Nowadays, TiO<sub>2</sub>  
73 has a large number of applications photocatalysis <sup>30-33</sup>, due to its high photocatalytic efficiency,  
74 stability under extreme conditions, and suitable edge potential to act as active centers for catalytic  
75 reactions <sup>34-36</sup>. However, the performance of these nano-catalyst is not efficient. For example,  
76 compared with other semiconductor materials, TiO<sub>2</sub> has a wider band gap and higher carrier  
77 recombination rate which limit the photocatalytic process to the UV region of the spectrum <sup>31, 37</sup>.

78 Recently, the techniques of modifying nano-catalyst include (i) the use of compound  
79 semiconductors i.e., semiconductors made from two or more elements, (ii) catalyst immobilization  
80 on solids such as silica or polymeric supports, (iii) use of co-catalysts, (iv) dye sensitization, and (v)  
81 surface doping is being applied to fill the shortcomings of nano-catalyst. These techniques not only  
82 enable catalyst to increase visible light utilization efficiency but also increase the lifetime of  
83 photoexcited carrier pairs <sup>38-42</sup>.

84 Previously published articles give a detailed introduction to the processes for modification of  
85 various nano-catalysts <sup>43-46</sup>. However, there is no comprehensive review on the impact of  
86 modification of nano-catalysts by the different methods on their efficiency and capability to  
87 eliminate VOCs. The purpose of this review is thus to classify the techniques according to the  
88 surface modification method and review the new features of the modified photocatalyst.  
89 Furthermore, new features of the modified photocatalyst are briefly discussed. Photocatalysis  
90 fundamentals, factors that affect the catalytic performance of the photocatalyst, and the modification

91 technology has been illustrated. Through these studies, we can explore the limitations of the current  
 92 catalysts and use this to further improve the performance of the catalysts, with the overarching goal  
 93 of contributing to the improved elimination of environmental VOC pollution by nano-catalysis in  
 94 the future.



95  
 96 **Fig 1. Illustration of industries releasing VOCs in air, concentration obtained from** 47-57.

97 **2. Mechanism behind photocatalytic oxidation of VOCs**

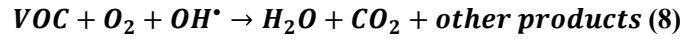
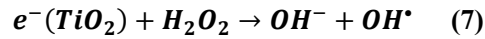
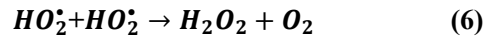
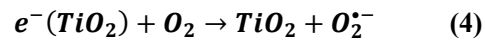
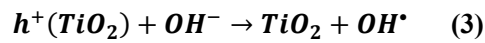
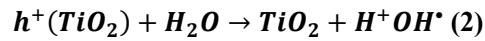
98 The photocatalytic reaction is a complex process, which begins with the absorption of a large  
 99 amount of visible light on the surface of the material. When the energy of the absorbed photon is  
 100 not less than the energy of the semiconductor band gap photon ( $E_g$ ), the electrons existing in valence  
 101 bands (VB) will be excited into the empty conduction bands (CB), such that holes are left behind in  
 102 the VB<sup>58</sup>. The following uses  $TiO_2$  as an example to analyze the electrons and holes generation  
 103 process:



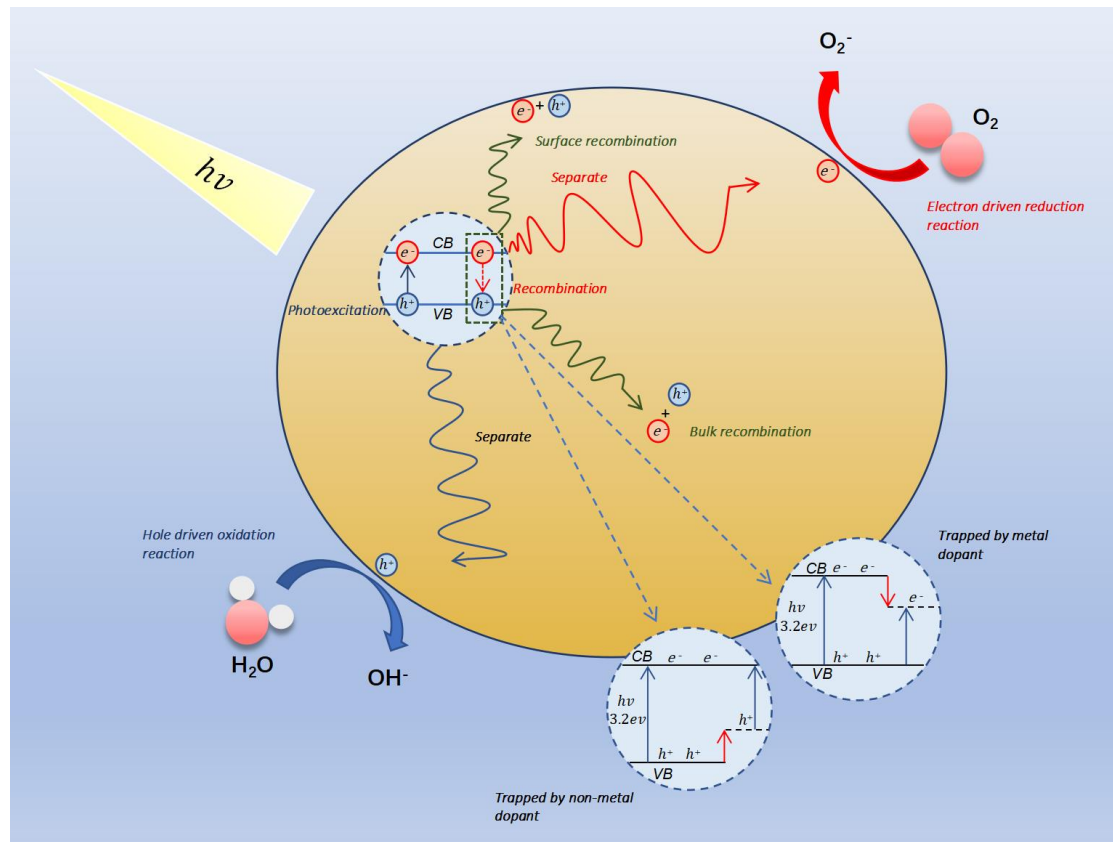
105 There are three possible processes for electrons and holes : (1) Separate and move to the surface  
 106 of the material to have an opportunity to participate in redox reaction (2) Trapped by defect sites.  
 107 (3) Recombine and release energy. However, the second and the third process do not promote the  
 108 photocatalytic reaction, and only the first process can drive reduction and oxidation<sup>59</sup>. Before  
 109 driving the redox reaction, the charge needs to undergo separation, thermalization, trapping,  
 110 recombination, and transport<sup>60</sup> (**Fig. 2**). Interfacial charge transfer may directly eliminate VOCs  
 111 through oxidation or generate hydroxyl radicals and superoxides<sup>61</sup>. The process can be depicted as  
 112 follows equations (2)-(8)<sup>62</sup>:

113  
 114  
 115  
 116  
 117  
 118

119  
120  
121  
122  
123  
124  
125  
126  
127  
128



Current model is difficult to explain due to the complex charge transfer process. Understanding the underlying mechanisms, will help us to find new photocatalysts for application in VOCs degradation.

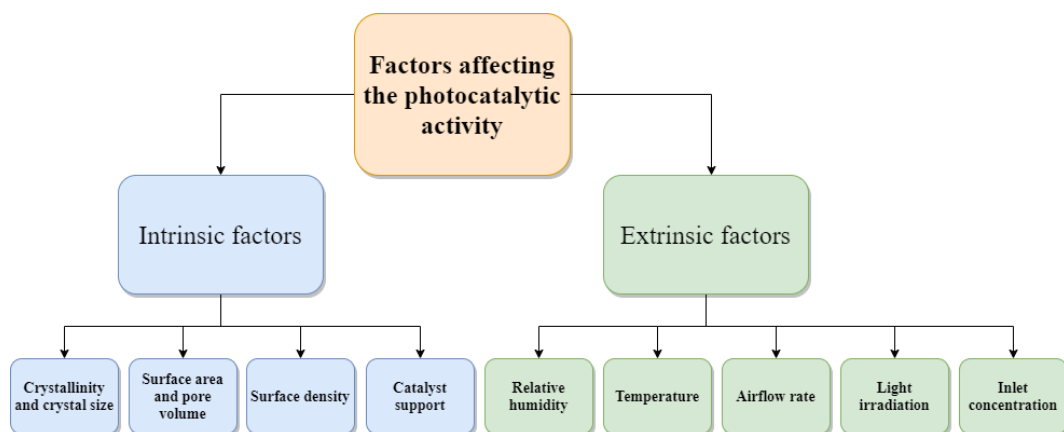


129  
130  
131  
132  
133  
134

**Fig 2. Schematic illustration of basic mechanism of photocatalysis.**

### 3. Factors affecting the photocatalytic activity

The photocatalytic performance affected by intrinsic and extrinsic factors (**Fig. 3**). Intrinsic factors affecting the photocatalytic ability and VOC degradation has been briefly discussed below



135  
136 **Fig 3. Illustration of factors affecting the photocatalytic activity.**

137 **3.1 Influence of catalyst characteristics (intrinsic factors) on VOCs degradation**

138 **3.1.1 Crystallinity and crystal size**

139 The presence of defects in crystal lattice and impurities in the catalyst accelerates the  
140 recombination process. To improve the efficiency of photocatalysis, the design and research of high  
141 bulk crystallinity have received extensive attention <sup>66</sup>.

142 Leite et al. <sup>67</sup>claimed that the property of high crystallinity has advantages over disordered  
143 polymers in photocatalytic applications. Pleskunov et al. <sup>68</sup>used a single-step plasma-based  
144 technique to synthesize Ta<sub>3</sub>N<sub>y</sub>O<sub>x</sub> nanoparticles(NPs) with controllable crystallinity. In the visible  
145 light range, Ta<sub>3</sub>N<sub>y</sub>O<sub>x</sub> exhibits plasmonic and photoluminescent properties. Katsuki et al. <sup>69</sup>found that  
146 α-Fe<sub>2</sub>O<sub>3</sub> NPs with high crystallinity are more efficient in PCO. A similar finding was also reported  
147 by Li et al. <sup>70</sup>, they found that the nanorod-shaped photoactive COF containing benzothiadiazole  
148 and triazine with good crystallinity exhibited excellent comprehensive performance and good cycle  
149 performance in the photocatalytic oxidation reaction. Curtis et al. <sup>71</sup>used the two-temperature  
150 method to prepare mesoporous silicon NPs. The initial temperature of the reaction is 650°C and  
151 lasted for 0.5h, and then in the second heating process at 100°C, 200°C and 300°C for 6h. They  
152 found that the mesoporous silicon NPs prepared at 300°C have the best photocatalytic performance  
153 because of the higher crystallinity of catalyst. Li et al. <sup>72</sup>and Zhang et al. <sup>73</sup> pointed out that  
154 synthesizing a new heterogeneous photocatalyst has uniform crystal size and high crystallinity.  
155 These advantages accelerate the separation and transfer efficiency of electron-hole pairs.

156 Besides crystallinity, crystal size also affects photocatalytic activity. Alonso-Tellez et al. <sup>74</sup> found  
157 that the smaller crystal size of UV100 is the main reason why it is superior to P25 in terms of  
158 photocatalytic oxidation. Generally speaking, higher crystallinity and smaller crystal size can  
159 promote the reaction rate.

160 **3.1.2 Surface area**

161 Surface area is an important structural feature of photocatalysts, which has a great influence on  
162 photocatalysis <sup>75</sup>. The larger surface area, the more accessible active sites, and the higher the  
163 photocatalytic efficiency <sup>76</sup>.

164 Hajaghadzadeh et al. <sup>77</sup>found that under steady-state conditions, the conversion rate of methyl

165 ethyl ketone (MEK) using PC500 catalyst was higher than that of PC50 and P25. The experimental  
166 results show that the lower surface area of PC50 and P25 makes the activity decrease over time.  
167 However, PC500 has a high surface area, and its positive impact offsets the negative impact of  
168 electron and holes on rapid recombination. This finding was also reported by Monteiro's group.  
169 During the degradation of perchloroethylene by P25 and PC500, it was also noticed that the surface  
170 area has a greater impact on the conversion of pollutants <sup>78</sup>. Liu et al. <sup>79</sup> found that Ag-ZnO NPs  
171 have super high photocatalytic efficiency compared with pure ZnO. Researchers speculate that it  
172 may be because the Ag NPs are uniformly distributed and have a large specific surface area. Similar  
173 results were also reflected in another experiment. Rajca's group tested the removal efficiency of  
174 organic substances in the photocatalytic process of commercial nano-catalysts with different  
175 accessible surface areas. The results show that because P90 has a larger surface area, the  
176 photocatalytic efficiency of P90 is higher than P25 <sup>80</sup>.

### 177 **3.1.3 Pore volume and porosity**

178 In addition to the surface area, another structural feature pore volume of the photocatalyst also  
179 has a profound effect on the catalytic efficiency<sup>74</sup>. Chen et al.<sup>81</sup> designed Pt nanoclusters similar to  
180 1.8 nm. The catalytic performance of C/Pt@TiO<sub>2</sub>-3% containing 0.54 wt% Pt is greatly improved  
181 because of its maximum total pore volume and the average pore diameter is approximately 3 nm. In  
182 addition, the mesoporous structure also helps to expose more active sites of the nano-catalyst to  
183 promote surface reactions <sup>81</sup>.

184 While achieving porous structure, crystallinity will not be lost. Therefore, the general view is  
185 that porous structure is more important catalyst characteristics than crystallinity <sup>62</sup>.

186 Porous materials with superior performance are very suitable for capturing aromatic VOCs in  
187 ambient air. In recent years, due to high porosity and strong customization, metal organic  
188 frameworks (MOFs) have been studied extensively <sup>82-86</sup>. MOFs are rich in organic contents, which  
189 makes them have superior inherent advantages in adsorbing aromatic VOCs <sup>87</sup>.

190 Xie et al. <sup>87</sup> designed and synthesized two MOFs, among which [Zr<sub>6</sub>(μ<sub>3</sub>-O)<sub>4</sub>(μ<sub>3</sub>-OH)<sub>4</sub>(BDB)<sub>6</sub>]  
191 (BUT-66) shows superior adsorption performance of benzene. Single-crystal structure analysis  
192 shows that the small hydrophobic pores and the small interaction between the adsorption sites make  
193 BUT-66 have the high performance of capturing benzene. Wu et al. <sup>88</sup> used lab-on-fiber technology  
194 and nanotechnology to monitor surface nano-functionalization of VOC adsorption/desorption in  
195 zeolitic imidazole frameworks (ZIF)-8. The high porosity plays an important role in VOC sensors.  
196 This finding was also reported by Wang et al. <sup>89</sup> They found that the shape and size of the porous  
197 Co<sub>3</sub>O<sub>4</sub> derived from Co-MOF would significantly affect its sensing performance. Besides, the more  
198 NPs on the surface, the better the VOC sensing performance. Yu et al. <sup>90</sup> proposed a two-step method  
199 to prepare In/Ni MOF-derived mesoporous In<sub>2</sub>O<sub>3</sub>-NiO composites with a nanosheet hollow sphere  
200 (NHS) structure. They observed that mesoporous In<sub>2</sub>O<sub>3</sub>-NiO NHS has a high porosity, this  
201 advantage provides sufficient permeation pathways for VOC, a large number of active sites, and the  
202 capacity to capture VOC.



203 Table 1 Summary of different photocatalysts affect the photoactivity

Photocatalyst	Surface area	Pore volume	Compound	Photo activity	Ref.
TiO <sub>2</sub> USprec	326 m <sup>2</sup> /g	0.484 cm <sup>3</sup> /g	Benzyl alcohol	Conversion 61%	91
P25	-	-	Benzyl alcohol	Conversion 100%	91
Brookite/anatase TiO <sub>2</sub> /g-C <sub>3</sub> N <sub>4</sub>	37.1 m <sup>2</sup> /g	0.2 cm <sup>3</sup> /g	Phenol	Degradation rate 5-fold increase over CN	92
CN	45.8 m <sup>2</sup> /g	0.29 cm <sup>3</sup> /g	Phenol	-	92
Ti <sup>3+</sup> doped TiO <sub>2</sub> /SiO <sub>2</sub>	300 m <sup>2</sup> /g	0.35 cm <sup>3</sup> /g	Methyl orange	31.5%	93
TiO <sub>2</sub>	56.8 m <sup>2</sup> /g	-	Methyl orange	8%	93
TiO <sub>2</sub> /SiO <sub>2</sub>	228 m <sup>2</sup> /g	0.27 cm <sup>3</sup> /g	Methyl orange	16.6%	93

204

205 **3.1.4 Surface density**

206 Surface density is a key factor as increasing the thickness of the nano-catalyst coating can  
 207 increase the surface area of the catalyst and reduce competitive adsorption between reactants,  
 208 thereby increasing the removal rate and the degree of mineralization of the catalyst <sup>94</sup>.

209 Singh et al. <sup>95</sup> used atomic layer deposition method coating TiO<sub>2</sub> on fibrous nanosilica (KCC-  
 210 1). They observed that the KCC-1/TiO<sub>2</sub> catalyst coated with TiO<sub>2</sub> NPs has a more uniform coating,  
 211 a higher loading of TiO<sub>2</sub>, a smaller loss of surface area, and higher active site accessibility than  
 212 traditional silica catalysts. Wang et al. <sup>96</sup> confined the dense Au nanoparticles to a bowl-shaped TiO<sub>2</sub>  
 213 nanoarray doped with N. By adjusting the absorption of light by TiO<sub>2</sub> and fully overlapping the  
 214 plasma band of Au NPs, the photocatalytic efficiency is greatly improved. Roldan et al. <sup>97</sup> researched  
 215 a new type of nanostructured coating system, which includes a layer of SiO<sub>2</sub> and a layer of dense  
 216 anatase TiO<sub>2</sub> doped with Ag NPs. The photocatalytic activity has been improved All in all,  
 217 increasing the surface density of the nano-catalyst can greatly increase the conversion of VOCs.  
 218 However, an excessive amount of catalyst will result in a decrease in catalytic efficiency.

219 **3.1.5 Support material**

220 Fixing the nano photocatalyst on a suitable carrier material can reduce their aggregation of the  
 221 NPs, thereby increasing the catalytic efficiency, adsorption capacity and prolonging the effective  
 222 life of the photocatalyst <sup>62</sup>. In recent years, engineered carbon has been applied to catalyst support  
 223 due to its high surface area, porous structure, high-performance adsorption of VOCs <sup>21</sup>. Activated  
 224 carbon (AC) has been applied to the adsorption and recovery of most VOCs. However, AC has some  
 225 shortcomings that affect its ability to adsorb VOCs: AC is an inherently non-polar adsorbent, which  
 226 will hinder the adsorption of hydrophilic particles <sup>22</sup>. Furthermore, the porous structure of activated

227 carbon is microporous (pore size < 2nm), which makes it difficult for molecules with larger  
228 molecular diameters to enter the pores. Furthermore, due to the strong diffusion resistance due to  
229 irregular pore structure, the adsorption equilibrium is prolonged due to the disordered pores  
230 possessed by AC. Zhang et al.<sup>98</sup> prepared a new nano- $\beta$ -FeOOH/Fe<sub>3</sub>O<sub>4</sub>/biochar composite material.  
231 Through XPS characterization, it is proved that there are Fe-OC bonds between  $\beta$ -FeOOH and  
232 biochar. These bonds facilitated the transfer of photo-generated electrons. The connection promotes  
233 the rapid interface transfer of light energy electrons between biochar and  $\beta$ -FeOOH. Zhang et al.<sup>99</sup>  
234 prepared N-doped nano-TiO<sub>2</sub>-carbon fiber composite material. After TiO<sub>2</sub> NPs are irradiated by  
235 microwaves, they generate a large number of hydroxyl adsorption sites. Due to the interface formed  
236 between TiO<sub>2</sub> and carbon fiber, this carbon fiber composite material can effectively catalyze the  
237 oxidation reaction of phenol. Graphene has the characteristics of inhibiting the annihilation of  
238 electrons and holes and exhibits excellent photoactivity, so it is widely used in photocatalysis<sup>100-102</sup>.  
239 Saima et al.<sup>103</sup> used graphene oxide(GO) as the support material and randomly dispersed TiO<sub>2</sub> and  
240 NiO NPS on it. The GO provides fast electronic conductivity and strong oxidation characteristics,  
241 which facilitates the separation of carriers.

242 As can be seen, the support material of the nano-catalyst will affect the removal of VOCs. In  
243 short, a suitable carrier can effectively increase the accessible surface area, mechanical strength and  
244 stability of the nano-catalyst.

### 245 **3.2 Effects of environmental conditions (external factors) on POC of VOCs**

246 The multi-factor synergistic mechanism of photocatalytic degradation of VOCs by adsorption  
247 is controlled by two aspects: thermodynamics and dynamics. Considering the complexity of the  
248 environment, we briefly review the effects of humidity, airflow rate, light irradiation, concentration  
249 of pollutants and temperature on the photocatalytic degradation of VOCs (**Fig. 4**). The factors  
250 influencing the comprehensive adsorption and photocatalysis capability of modified NMs are  
251 discussed in **Table 2**.

252

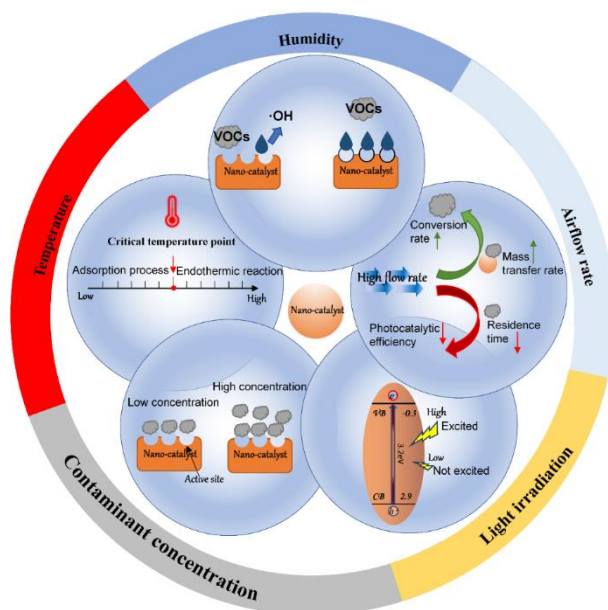


**Fig 4. Illustration of external factors and mechanism of action.**

### 3.2.1 Relative humidity and temperature

Water vapor plays a double-sided role in the process of photocatalysis of VOCs and their adsorption onto/interactions with modified NMs<sup>104, 105</sup>. As a polar molecule, water can provide hydroxyl radicals, which is conducive to the adsorption of more hydrophilic VOCs molecules onto the photocatalyst surface through hydrogen bonds. However, if the moisture content is too high, it will compete with VOCs for the adsorption sites. For some pollutants, the presence of moisture can promote mineralization of the pollutants, but excessive moisture will be adsorbed onto the active sites of the catalyst, thereby reducing the catalytic efficiency of the catalyst<sup>106</sup>. Regarding air humidity, modification of the nano-catalyst can reduce the degree of competition between water molecules and VOCs; for example, doped TiO<sub>2</sub> has a higher catalytic efficiency than undoped TiO<sub>2</sub> because the introduction of dopants resulting in more oxidant<sup>107-111</sup>.

Temperature is another key factor affecting photocatalysis. In the adsorption process of VOCs onto the photocatalytic material, low temperature is conducive to adsorption processes dominated by exothermic reactions, but it reduces the diffusion rate of adsorbate molecules. Huang et al.<sup>112</sup> pointed out that the efficiency of PCO of formaldehyde is higher at 60°C than at 30°C. This phenomenon shows that higher temperature promotes the photocatalytic process. At lower temperatures, the VOC adsorption process is dominant, and the rate is higher than the photocatalytic oxidation rate<sup>113</sup>.

### 3.2.2 Airflow rate and contaminant concentration

The airflow rate affects the photocatalytic oxidation process of VOCs, and similar to temperature bring advantages and disadvantages. Increasing the airflow rate will increase the transfer rate of VOCs and increase the conversion rate of pollutants. On the contrary, too high air flow rate will reduce the residence time of VOCs and thus reduce the photodegradation efficiency<sup>114-116</sup>. Therefore, optimizing the air flow rate is essential: low air flow rate can increase the residence

279 time of VOCs so that they can be fully adsorbed on the catalyst surface. Under high flow rates, the  
280 residence time is reduced so the removal rate will be reduced. Thus, flow rate should be optimized  
281 for each catalyst-VOC pair to determine the optimal flow rate and maximize the PCO efficiency.

282 The adsorption capacity of the catalyst is related to the number of active sites. When the  
283 concentration of VOCs is low (located in the appropriate range) and the adsorption capacity can  
284 meet the adsorption demand, the removal efficiency will be improved. Since the by-products  
285 produced by catalysis compete for adsorption sites, PCO is more suitable for the degradation of low  
286 concentration pollutants<sup>117, 118</sup>. An area for future development is a means to remove the by-products  
287 from the adsorption sites, or to ensure they have a lower binding affinity for the sites than the target  
288 VOC pollutants.

### 289 **3.2.3 Light irradiation**

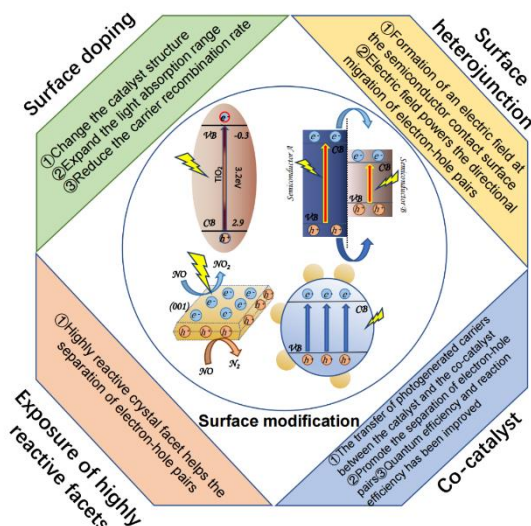
290 It is worth mentioning that light irradiation (wavelength and intensity of light) has a greater  
291 impact on the photocatalytic process than adsorption process. On the one hand, the wavelength of  
292 light is related to  $E_g$  and the energy of the band gap photon. If  $E_g$  is too low (less than the energy  
293 band of the catalyst) so that the electrons will not be excited and the oxidation process of VOCs on  
294 the catalyst surface is difficult to occur. On the other hand, under low light intensity conditions, the  
295 light intensity is related to the photocatalytic rate, and as the light intensity increases, the rate and  
296 light intensity show a power-law relationship<sup>119</sup>. However, in PCO, the energy loss caused by light  
297 reflection and transmission is inevitable. Therefore, researchers have used modification methods  
298 such as doping, use of compound semiconductor, and surface modification to use energy as much  
299 as possible<sup>106, 120-122</sup>.

300 Table 2 The key factors affecting VOC photocatalytic performances.

Factors	VOCs	Humidity	Temperature	Airflow rate	Light	Inlet concentration	Removal efficiency	Ref.
			e					
Humidity	MEK	0%	23 ± 1 °C	0.015 m <sup>3</sup> /min	UV	2.65 ± 0.3 mg/m <sup>3</sup>	41%	123
		20%					46%	
		40%					44%	
		60 ± 1%					41%	
	2-ethyl-1-hexanol	20%	-	-	visible light	0.1 ppm	89%	124
		50%					85%	
		80%					70%	
Temperature	toluene	-	155-160 °C	30,000mL/g h	650mW/cm <sup>2</sup>	200ppm	40-50%	125
			220-230 °C				90-95%	
	toluene	-	130°C	40,000mL/g h	-	-	18-20%	126
			180°C				57-60%	
Airflow rate	acetaldehyde	20 ± 1%	25°C	20L/min 40L/min	UV lamps	15 ppm	35-40% 20%	127
Light	MEK	0%	23 ± 1 °C	0.015 m <sup>3</sup> /min	UV	2.65 ± 0.3 mg/m <sup>3</sup>	60-70%	123
			24 ± 2 °C		visible light		40-50%	
	1-propanol	10%	30 °C	320 mL/min	1.0 mW/cm <sup>2</sup> 2.0 mW/cm <sup>2</sup> 3.0 mW/cm <sup>2</sup>	400 ppm	45% 55% 65%	110
Inlet concentration	toluene	-	-	-	visible light	115 ppm	100%	128
						230 ppm	100%	
						460 ppm	87.1%	
						690 ppm	65.5%	

302 **4. Surface modification of nano-catalysts as a means to increase PCO efficiency for VOCs**

303 The intrinsic properties of the nanomaterial photocatalysts and the extrinsic factors effecting  
304 nano-catalysts have significant role on photocatalytic efficiency. Surface modification methods  
305 investigated to date include surface doping, the structure of surface heterojunctions, utilizing a  
306 supported co-catalyst, increasing the surface area, and ensuring high reaction surface exposure (**Fig.**  
307 **5**). These are discussed below.



308

309 **Fig 5. Schematic illustration of different surface modification methods effect on**  
310 **photocatalytic efficiency.**

311 **4.1 Surface doping**

312 Surface doping can introduce electrons into the band gap of semiconductor, causing an optical  
313 response, which in turn produces a significant redshift. This two-step light excitation process excited  
314 by low-energy visible photons promote the visible light activity of the semiconductor <sup>129</sup>. By doping  
315 with metal elements, Fang et al. <sup>130</sup> found that surface doping significantly improves the catalytic  
316 efficiency of the catalyst for refractory benzene. However, the lattice defects caused by doping can  
317 not only serve as the transfer medium of the interface charge but also become the complex center of  
318 electron-hole pairs, reducing the catalytic activity <sup>129, 131</sup>. In addition to a single doped metal or non-  
319 metal element, co-doping between metal ions, non-metal elements, or between metal ions and non-  
320 metal elements can also effectively extend the wavelength of the photocatalyst excitation light.

321 **4.1.1 Metal doping**

322 At present, the research on doping of metal elements mainly includes noble metals, transition  
323 metals and rare earth metals. However, noble metals cannot be widely used in practice due to their  
324 high cost and scarcity of raw materials. Exploring the effects of different metal doping on  
325 photoactivity, optimal doping dose and preparing nano-catalysts with the best benefits and efficiency  
326 has become the focus of current research (**Fig. 6**).

327 Generally, the preparation method of the doped catalyst will produce different crystal properties

328 and change the morphology of the photocatalyst. The mechanism behind metal doping can be  
329 summarized as follows: (1) Noble metals have anti-oxidation and corrosion resistance properties  
330 even in humid air. Under the action of noble metal NPs, the recombination of carriers is reduced,  
331 which increases the photoactivity on the surface of the photocatalyst. (2) The type and doping  
332 amount of transition metals are two key factors that affect the PCO. If the doping amount is at the  
333 optimal value, the dopant can accelerate the separation of carriers. When the optimal value is  
334 exceeded, the dopant may become a recombination center, reducing the photocatalytic efficiency.  
335 (3) Rare earth metals have incomplete 4f and empty 5d orbitals, which can promote photocatalytic  
336 reactions.

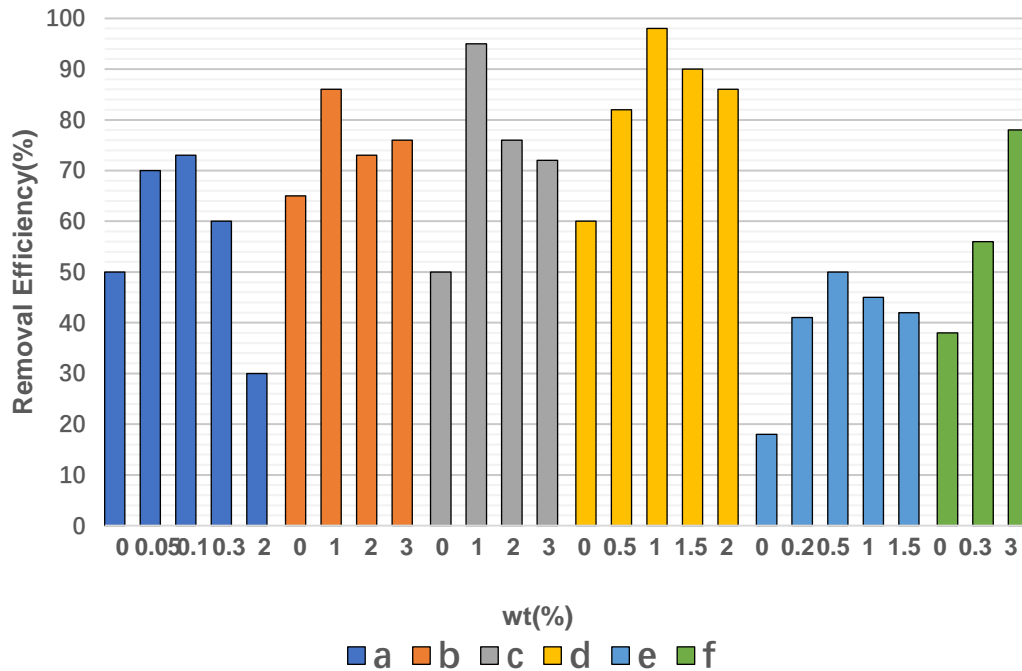
337 Noble metal elements such as platinum (Pt)<sup>132</sup>, palladium (Pd)<sup>133</sup>, ruthenium (Ru)<sup>134</sup>, silver  
338 (Ag)<sup>135</sup>. Because of noble metals, the recombination of carriers is reduced, which improve the  
339 photoactivity of the catalyst<sup>136</sup>. In fact, the doping of noble metal NPs forms a medium for capturing  
340 and transferring electrons on the nano-catalyst surface<sup>137</sup>. Meng et al.<sup>138</sup> doped Pd/PdCl<sub>2</sub> onto the  
341 surface of the nano-catalyst Bi<sub>2</sub>WO<sub>6</sub> by photoreduction method. Compared with TiO<sub>2</sub>, the catalyst  
342 degrades phenol more efficiently. The researchers concluded that it may be due to the dual factors  
343 of the plasmon resonance and the suppression of photo-generated carrier recombination. Xue et al.<sup>139</sup>,  
344 modified TiO<sub>2</sub> doped with Ag and Ag<sub>2</sub>O. The efficiency of this catalyst to degrade toluene is 50%,  
345 which is about 9.7 times higher than TiO<sub>2</sub>.

346 Transition metal doping can significantly extend visible light excitation, and more susceptible  
347 to doping by other transition metals because of the lower energy required for the substitution process.  
348 Thus, there has been extensive research on transition metal doping, such as manganese (Mn)<sup>140, 141</sup>,  
349 iron (Fe)<sup>142-144</sup>, copper (Cu)<sup>145</sup>, vanadium (V)<sup>146, 147</sup>, and nickel (Ni)<sup>148</sup>. Afif et al.<sup>149</sup> successfully  
350 synthesized a highly active Mn-doped Ag<sub>3</sub>PO<sub>4</sub> photocatalyst using the co-precipitation method. Mn  
351 doping suppressed hydroxyl defects and oxygen vacancies, increased the atomic ratio of oxygen to  
352 silver, and improved the photocatalytic performance under visible light irradiation. Patrick et al.<sup>150</sup>  
353 found that the photochemical properties of the Mn complex reached or approached the performance  
354 of Ru and Ir noble metal catalysts in terms of photon absorption. Devaraji group<sup>151</sup> incorporated V  
355 into the TiO<sub>2</sub> crystal lattice to make Ti<sub>0.98</sub>V<sub>0.02</sub>O<sub>2</sub>. Compared with pure TiO<sub>2</sub>, this catalyst embodies  
356 the quantum transition of benzene oxidation, highlighting the importance of V doping for benzene  
357 oxidation. Stucchi et al.<sup>152</sup> used Mn to replace noble metals such as Au and Ag. Through  
358 experiments, it was found that TiO<sub>2</sub> doped with 20% Mn under visible light exposure for 24 h, the  
359 degradation efficiency of ethanol reached 35%, which is the peak degradation efficiency. The  
360 suppression of the defect sites on the catalyst surface and the reduction of electrons compound with  
361 holes that may be the reasons for the excellent photocatalytic activity. Li et al.<sup>153</sup> prepared Co-doped  
362 TiO<sub>2</sub> nanorod array (Co-TiO<sub>2</sub> @Ti(H<sub>2</sub>)) with good stability, and the energy barrier for desorption  
363 can be effectively reduced by introducing Co with abundant oxygen vacancies. Sajjad et al.<sup>154</sup> used  
364 Si and Ti to modify the magnetic Fe<sub>3</sub>O<sub>4</sub> NPs. It was found that the photodegradation effect was in  
365 the order of Ti modified Fe<sub>3</sub>O<sub>4</sub>>Si modified Fe<sub>3</sub>O<sub>4</sub>>Fe<sub>3</sub>O<sub>4</sub>.

366           There are 17 kinds of lanthanides, collectively referred to as rare earth metals. Kumar et al. <sup>39</sup>  
367 found that lanthanide ion dopants are beneficial to the optical properties of ZnO structure.  
368 Parameters such as material properties and pollutant degradation reaction conditions have influence  
369 on the performance of ZnO. Xiao et al. <sup>155</sup>found that Ce-doped TiO<sub>2</sub> shows the advantages of  
370 stability and higher surface area. Notable, the adsorption capacity of VOCs is also greatly enhanced.  
371 The same result also appeared in other experiments. Wang et al. <sup>156</sup> synthesized Ce-doped MoS<sub>2</sub>  
372 nanocomposite by hydrothermal method. Under visible light irradiation, it exhibits excellent  
373 photocatalytic activity.

374           It is worth noting that different cationic dopants have individual effects on the nano-catalyst.  
375 Generally speaking, metal doping will produce different properties and also affect the morphology  
376 of the nano-catalyst. The lattice defects caused by doping may become the recombination center of  
377 carriers, thereby reducing the catalytic activity. Therefore, searching for the optimal amount of  
378 doping is still the focus of future work.





379

380 **Fig 6. The effect of different doping amounts on the degradation of VOCs by photocatalyst.**

381 **(a) acetaminophen, Sb-doped TiO<sub>2</sub><sup>157</sup>. (b) 4-chlorophenol, W-doped TiO<sub>2</sub><sup>158</sup>. (c) 4-**

382 **chlorophenol, Mo-doped TiO<sub>2</sub><sup>158</sup>. (d) 2,4-dichlorophenol, Ce-doped CuMgAl<sup>159</sup>. (e) MEK,**

383 **Ce-TiO<sub>2</sub><sup>160</sup>. (f) acetaldehyde, Cr-TiO<sub>2</sub><sup>161</sup>.**

384

#### 385 4.1.2 Non-metal doping

386 Non-metal doping such as nitrogen (N)<sup>162-166</sup>, carbon (C)<sup>167-169</sup>, sulfur (S)<sup>170-173</sup>, boron (B)<sup>174,</sup>

387 <sup>175</sup>and fluorine (F)<sup>176</sup> has been extensively evaluated previously. In non-metal doping, dopants can

388 change the morphology and improve photoactive performance of the catalyst. Because the doped

389 state is close to the edge of VB and is not used as a carrier, the role of the recombination center will

390 be weakened. When the oxygen atom is replaced by other non-metal element atoms, the top energy

391 level of the VB of the oxide will increase, and the semiconductor band gap will be narrowed, thereby

392 extending the excitation wavelength to improve catalytic efficiency.

393 Table 3 summarizes metal and non-metal doped photocatalysts synthesized to improve

394 photocatalytic degradation performance. A conclusion can be drawn that after doping, the catalytic

395 efficiency of the catalyst has been improved.

396

397

398

399

400

401

402

403 Table 3. Summary of metal and non-metal doped photocatalysts.

Contaminant	Photocatalyst	Dopant	Efficiency before doping	Efficiency after doping	Ref.
Toluene	TiO <sub>2</sub>	Ag/Ag <sub>2</sub> O	7.5%	23.3%	139
Benzene	OMS-2	Mg	68.4%	97.2%	130
Benzene	TiO <sub>2</sub>	V	0.3%	12.7%	151
Benzene	Ti <sub>0.98</sub> V <sub>0.02</sub> O <sub>2</sub>	Au	9%	18%	151
Acetaldehyde	TiO <sub>2</sub>	F	77.3%	81%	177
Acetaldehyde	TiO <sub>2</sub>	N	77.3%	92.1%	177
Ethylbenzene	TiO <sub>2</sub>	N	33%	38%	178

404 Awin et al.<sup>179</sup> pointed out that the N-doped TiO<sub>2</sub> on the Si-OCN support exhibited excellent  
 405 adsorption properties and high catalytic activity under visible light. Sun et al.<sup>180</sup> developed C-doped  
 406 and oxygen vacancies Bi<sub>2</sub>WO<sub>6</sub> nanospheres mediated by graphene oxide. C-doping can change the  
 407 band gap structure and can also promote light absorption. This is because carbon doping in the  
 408 catalyst acts as an acceptor and electron channel to promote the separation of carriers and the  
 409 production of active substances. Diao et al.<sup>181</sup> synthesized F-doped TiO<sub>2</sub> by hydrothermal method  
 410 and used EPR measurements to prove that F-doped TiO<sub>2</sub> has superior degradability to formaldehyde  
 411 due to the participation of superoxide radical and hydroxyl radical in the process of oxidizing  
 412 formaldehyde into CO<sub>2</sub> and H<sub>2</sub>O. Ramacharyulu et al.<sup>182</sup> noted that compared with undoped TiO<sub>2</sub>,  
 413 S-doped TiO<sub>2</sub> had a lower band gap value and better photocatalytic activity. Among various doping  
 414 materials, non-metallic element doping has been tested to be a better way to improve PCO activity<sup>183</sup>,  
 415 <sup>184</sup>.

#### 416 4.2 Structure of surface heterojunction

417 When two semiconductors with similar characteristics are in contact, an electric field is formed  
 418 at the contact interface. The electric field provides the driving force for the directional migration of  
 419 electron-hole pairs between different semiconductors, which can promote the effective separation.  
 420 This promotes the oxidation-reduction reaction of the nano-catalyst, which in turn facilitates the  
 421 degradation of VOC. In heterojunction photocatalysis, photogenerated electrons generally migrate  
 422 from a semiconductor with a higher CB energy level, and a photogenerated hole will migrate from  
 423 a semiconductor with a lower VB energy level. The mechanism of surface heterojunction is that a  
 424 well-defined junction can effectively promote charge transfer and hinder the recombination of  
 425 electrons and holes. Thus nano-catalysts shows high activity and stability.

426 Table 4 shows surface heterojunction effect photoactivity. Obviously, the formation of  
 427 heterojunction promotes the degradation efficiency of pollutants.

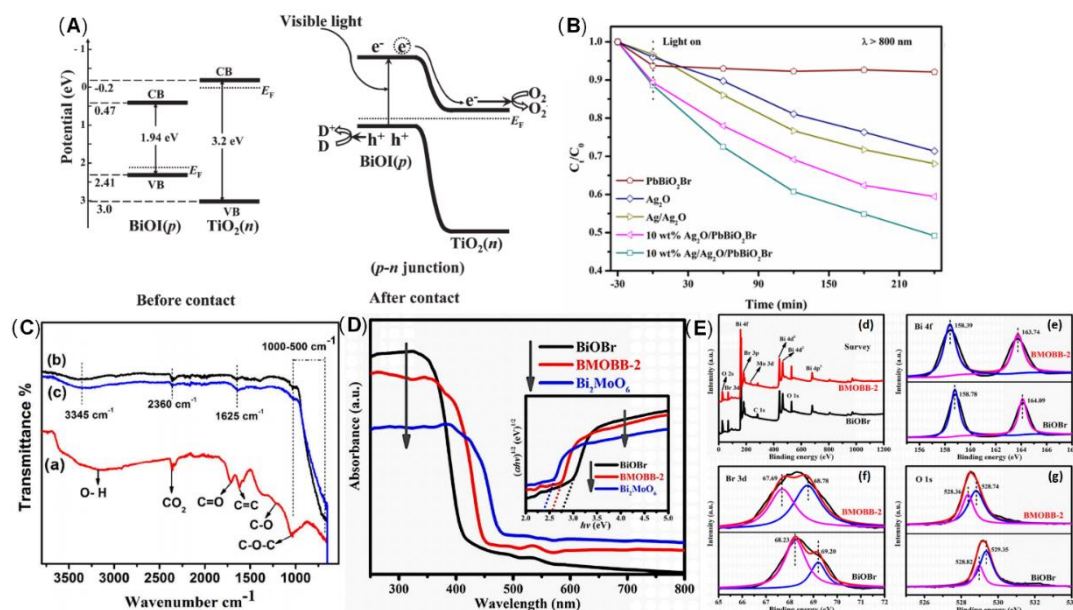
428  
 429  
 430  
 431

432 Table 4. Heterostructure and degradation efficiency of photocatalyst.

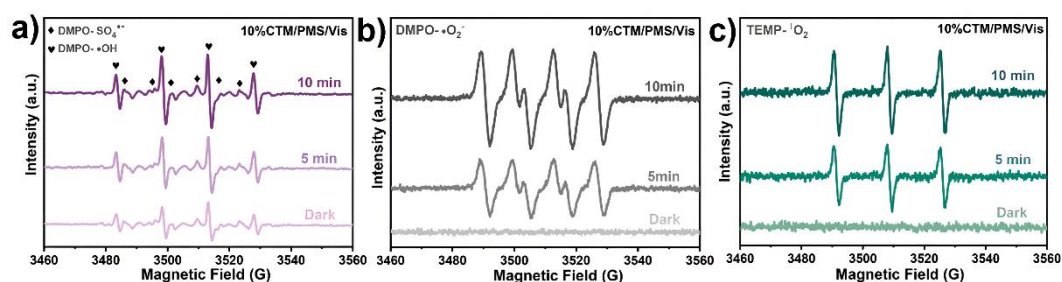
Heterostructure	Photocatalyst	Efficiency before	Efficiency after	Ref.
Z-Scheme	LaFeO <sub>3</sub> /g-C <sub>3</sub> N <sub>4</sub>	37%	100%	185
Z-Scheme	Au-TiO <sub>2</sub> @NH <sub>2</sub> - UiO-66	10%	85%	186
S-scheme	Cu <sub>2</sub> S/SnO <sub>2</sub>	17.9	67.2%	187

433

434 Dai et al.<sup>188</sup> used a new hydroxylation method to coat BiOI on the TiO<sub>2</sub> wall to form the p-n  
435 junction of the BiOI/TiO<sub>2</sub> nanotube array (**Fig. 7A**). They found the photo-electrocatalytic  
436 degradation efficiency of BiOI/TiO<sub>2</sub> was increased by 3 times. Guo et al.<sup>189</sup> successfully prepared  
437 an Ag/Ag<sub>2</sub>O/PbBiO<sub>2</sub>Br photocatalyst with a broader spectral response through a series of plasma p-  
438 n heterojunctions. Researchers have observed significantly accelerated charge separation, and the  
439 degradation efficiency of pollutants has also been significantly improved (**Fig. 7B**). Huang et al.<sup>190</sup>  
440 developed the p-n junction BiOI@Bi<sub>12</sub>O<sub>17</sub>Cl<sub>2</sub> heterostructure by depositing BiOI nanosheets in situ.  
441 Due to charge induction, BiOI@Bi<sub>12</sub>O<sub>17</sub>Cl<sub>2</sub> forms a unique front-side coupling heterostructure.  
442 Compared with the pure sample, the obtained BiOI@Bi<sub>12</sub>O<sub>17</sub>Cl<sub>2</sub> heterostructure can significantly  
443 enhance the catalytic performance and degradation of 2,4-Dichlorophenol. Anum et al.<sup>191</sup> studied a  
444 new type heterojunction of Al<sub>2</sub>O<sub>3</sub> and GO. FTIR examination showed that the density of hydroxyl  
445 on the surface of pure Al<sub>2</sub>O<sub>3</sub> was lower, but after adding GO, the density increased (**Fig. 7C**). The  
446 reason may be related to the interaction between hydroxyl and light-generated holes, which  
447 promotes electron transfer and inhibits the recombination of carriers. Because of GO, the  
448 recombination of electron-hole pairs is reduced. Through the study of activity, it was found that  
449 15.0% GO/Al<sub>2</sub>O<sub>3</sub> exhibits superior photocatalytic performance. In another study, the same result  
450 was observed<sup>192</sup>. Wu et al.<sup>185</sup> constructed a new p-type LaFeO<sub>3</sub> microspheres coated with n-type  
451 nano-scale graphite carbon nitride nanosheets. The interface effect of charge carriers is separated  
452 and transferred more effectively through solid p-n heterojunction. Yao et al.<sup>193</sup> prepared p-n  
453 heterojunction of Bi<sub>2</sub>MoO<sub>6</sub>/BiOBr which can promote the photocatalysis. In addition the UV-vis  
454 absorption edge of the BMOBB-2(The mole ratio of Na<sub>2</sub>MoO<sub>4</sub>·2H<sub>2</sub>O to Bi(NO<sub>3</sub>)<sub>3</sub>·5H<sub>2</sub>O is set as  
455 5%) sample has a significant red shift, which is related to the better visible light response of  
456 Bi<sub>2</sub>MoO<sub>6</sub>(**Fig. 7D**). Due to the strong interaction between BiOBr and Bi<sub>2</sub>MoO<sub>6</sub>, the binding energy  
457 changes in the XPS spectrum. It can be seen that there are carrier transfer and chemical bonds at the  
458 heterojunction interface between BiOBr and Bi<sub>2</sub>MoO<sub>6</sub>(**Fig. 7E**). Another study concluded that the  
459 Z-type heterojunction is the main reason for improving the photocatalytic performance of  
460 Ag<sub>3</sub>PO<sub>4</sub>/Ag/MoS<sub>2</sub>/TiO<sub>2</sub> composites<sup>194</sup>. Wang et al.<sup>195</sup> developed an electrochemically self-doped  
461 WO<sub>3</sub>/TiO<sub>2</sub> nanotube-composite film by doping oxygen vacancies into heterojunctions for  
462 photocatalytic degradation of exhaust gas. Ding et al.<sup>196</sup> synthesized a CoO@TiO<sub>2</sub>/MXene hybrid  
463 with a double heterojunction structure. EPR measurements prove that SO<sub>4</sub><sup>·-</sup>, ·O<sub>2</sub><sup>-</sup> and <sup>1</sup>O<sub>2</sub> are the  
464 main reactive species involved in the photocatalytic degradation of phenol (**Fig. 8**).



465  
 466 **Fig 7. (A) Schematic diagrams of the energy bands of p-BiOI and n-TiO<sub>2</sub> before light**  
 467 **irradiation and formation of a p-n junction under visible light irradiation. Adapted with**  
 468 **permission from ref.<sup>188</sup>. Copyright 2011, American Chemical Society. (B) Photocatalytic**  
 469 **degradation of tetracycline with obtained samples under NIR light ( $\lambda > 800$ nm). Adapted with**  
 470 **permission from ref.<sup>189</sup>. Copyright 2019, Elsevier. (C) FTIR spectra of various samples; (a)**  
 471 **pure GO (b) pure  $\gamma$ -Al<sub>2</sub>O<sub>3</sub> (c) 10.0% GO/Al<sub>2</sub>O<sub>3</sub> composite. Adapted with permission from**  
 472 **ref.<sup>191</sup>. Copyright 2018, American Chemical Society. (D) UV-vis diffuse reflectance spectra**  
 473 **(DRS). Adapted with permission from ref.<sup>193</sup>. Copyright 2021, Elsevier. (E) (d) XPS survey**  
 474 **spectra and high resolution XPS spectra of (e) Bi 4f, (f) Br 3d, (g) O 1s of BiOBr and**  
 475 **BMOBB-2. Adapted with permission from ref.<sup>193</sup>. Copyright 2021, Elsevier.**



476  
 477 **Fig 8. EPR spectra of 10%CTM/PMS/Vis system for (a) 5,5-Dimethyl-1-pyrroline N-oxide**  
 478 **(DMPO)-  $\bullet$ OH and DMPO-  $\text{SO}_4^{\bullet-}$ , (b) DMPO-  $\text{O}_2^{\bullet-}$  and (c) TEMP-  $^1\text{O}_2$ . Adapted with**  
 479 **permission from ref.<sup>196</sup>. Copyright 2021, Elsevier.**

#### 480 4.3 Supported co-catalyst

481 The electron-hole transfer between co-catalyst and semiconductor not only accelerates the  
 482 separation of carriers but also realizes the spatial separation of oxidation and reduction reactions so  
 483 that both quantum efficiency and reaction efficiency are improved. In addition, the co-catalyst also  
 484 has abundant surface active sites, which can cut back the overpotential of the surface reaction,  
 485 thereby increasing the surface reaction rate.

486 Wang et al.<sup>197</sup> found that WSe<sub>2</sub>/g-C<sub>3</sub>N<sub>4</sub> prepared with WSe<sub>2</sub> as a co-catalyst both promotes  
487 light absorption and improves charge transfer efficiency. Peng et al.<sup>161</sup> by comparing the amount of  
488 co-catalyst, found that the Cr<sub>x</sub>O co-catalyst (3wt%) is beneficial to improve the removal efficiency  
489 of acetaldehyde. Shen et al.<sup>198</sup> used the organic molecule oxamide (OA) as a co-catalyst to prepare  
490 modified TiO<sub>2</sub> samples through wet chemical methods to enhance electron-hole separation and  
491 photocatalytic H<sub>2</sub> precipitation on TiO<sub>2</sub>. Bai et al.<sup>199</sup> found that MoS<sub>2</sub> as a TiO<sub>2</sub> co-catalyst has the  
492 following characteristics: (1) No noble metals; (2) High charge transport mobility; (3) Many active  
493 sites.

#### 494 **4.4 Exposure of highly reactive facets**

495 Crystals have different optical and electronic structures, so the crystals have unique properties,  
496 such as adsorption, high activity and selectivity. The crystal facet can also promote the separation  
497 of electrons and holes. Furthermore, the reactivity physical and chemical properties of surface facets  
498 are also critical to determine its workability<sup>200</sup>.

499 Liang et al.<sup>201</sup> prepared a high proportion of active (002) crystal planes (>90%) and high  
500 specific surface area ultra-thin WO<sub>3</sub> nanosheets, which improved the performance of the catalyst to  
501 degrade pollutants. Yu et al.<sup>202</sup> synthesized TiO<sub>2</sub> nanosheets. The exposed (001) crystal facets are  
502 beneficial for the reduction of NO<sub>x</sub>. The NO conversion rate of the hydrothermal method prepared  
503 TiO<sub>2</sub> sheets is higher than the conversion rate of commercial P25 and TiO<sub>2</sub> particles synthesized by  
504 the sol-gel method. Li et al.<sup>203</sup> prepared Z-scheme rGO/Bi<sub>2</sub>S<sub>3</sub>-BiOBr heterojunction which has  
505 adjustable exposed BiOBr (102) crystal facet. The optimized catalyst has the best photocatalytic  
506 oxidation performance in a single system, and the degradation efficiency of 2-nitrophenol reaches  
507 92%. In different photocatalytic applications, the crystal facets promote the separation of carriers,  
508 exposing the highly reactive facets to improve the activity of the catalyst has become a promising  
509 method.

#### 510 **5. Summary and outlook**

511 Rapid economic development has posed serious environment and health problems coming  
512 from VOCs. They come from a wide range of sources and can cause diseases and even  
513 carcinogenesis in the human body. In addition, under light exposure, VOCs generate photochemical  
514 smog, and certain halogenated hydrocarbons can cause the destruction of the ozone layer. Up to date,  
515 photocatalysis is being recognized as an effective and clean treatment method for VOC removal as  
516 it operates at room-temperature, produce no secondary pollution, and have high removal activity.  
517 Furthermore, the photocatalytic efficiency has been greatly improved by surface modification of the  
518 nano-catalysts.

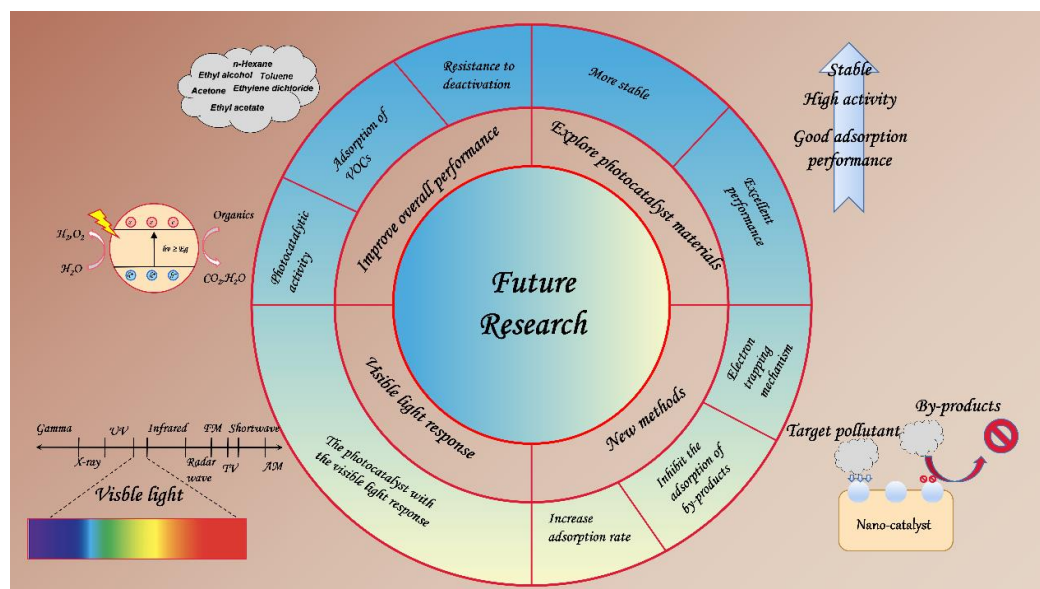
519 In this work, we reviewed the influence mechanism of the intrinsic and extrinsic factors of  
520 nano-catalysts on the catalytic degradation of VOCs. In addition, four nano-catalyst surface  
521 modification strategies are also discussed: surface doping, surface heterojunction, co-catalyst and  
522 exposure of highly reactive crystal facets. And analyze and evaluate these four methods respectively.

523 From what was discussed, the following conclusions can be drawn: (1) By understanding the

524 basic principles of photocatalysis, it was found that surface modification of the photocatalyst can  
 525 reduce the recombination of the carrier and improve the photoactivity of the nano-catalyst. (2) The  
 526 morphology of the catalyst affects the adsorption of VOCs, and the high surface area and porous  
 527 structure are conducive to the adsorption of VOCs. (3) Temperature and humidity will seriously  
 528 affect the adsorption of VOC. Low temperature is conducive to adsorption processes dominated by  
 529 exothermic reactions. High humidity will reduce the adsorption capacity of VOCs. However,  
 530 photocatalysis also has shortcomings: (1) The photocatalysis is limited to the treatment of low  
 531 concentrations of pollutants. (2) The performance of the photocatalyst is affected by internal and  
 532 external factors. (3) The lattice defects caused by doping can reduce the catalytic activity. Therefore,  
 533 there is often an optimal amount of doping.

534 Based on our current knowledge about the limitations of PCO technology in removing VOCs,  
 535 we can make some suggestions for future research (**Fig. 9**): (1) Improve the electronic and chemical  
 536 properties of the nano-catalyst to improve its photocatalytic activity, adsorption of VOCs and  
 537 resistance to deactivation. (2) Explore more stable and more efficient photocatalyst materials,  
 538 combining different strategies such as facets, heterojunctions and co-catalysts. (3) Photocatalysts  
 539 with the visible light response show enormous promise and should be widely researched. (4) More  
 540 attention should be paid to development of synthesis methods that contribute to electron trapping  
 541 mechanism, efficient structures and production methods. (5) Increase the rate of adsorption and  
 542 reduce the competitive adsorption behavior of by-products.

543 We hope that the presented overview can provide key research progress in the field of  
 544 photocatalysis of the modified NMs, and expect to making greater progress in the design of nano-  
 545 catalysts in the near future.



546  
 547

**Fig 9. Prospects for future research.**

548 **Author contributions**

549 Weichen Zhao: Writing - Original Draft, Visualization, Conceptualization. Muhammad Adeel:  
550 Writing - Review & Editing, Conceptualization. Peng Zhang, Pingfan Zhou, Lli Huang, Yongwen  
551 Zhao, Muhammad Arslan Ahmad, Noman Shakoor, Benzhen Lou, Yaqi Jiang, Iseult Lynch: Writing  
552 - Review & Editing. Yukui Rui: Writing - Review & Editing, Supervision.

553 **Declaration of Competing Interest**

554 The authors declare that they have no known competing financial interests or personal relationships  
555 that could have appeared to influence the work reported in this paper.

556 **Acknowledgements**

557 The project was supported by National Key R&D Program of China (2017YFD0801300,  
558 2017YFD0801103), National Natural Science Foundation of China (No. 41130526), Professor  
559 workstation in Yuhuangmiao Town, Shanghe County, China Agricultural University and Professor  
560 workstation in Sunji Town, Shanghe County, China Agricultural University.

561 **References**

- 562 1. P. Amoatey, H. Omidvarborna, M. S. Baawain and A. Al-Mamun, Emissions and exposure  
563 assessments of SOX, NOX, PM10/2.5 and trace metals from oil industries: A review study (2000-  
564 2018), *Process Saf. Environ. Protect.*, 2019, **123**, 215-228.
- 565 2. B. B. Huang, C. Lei, C. H. Wei and G. M. Zeng, Chlorinated volatile organic compounds (Cl-VOCs)  
566 in environment - sources, potential human health impacts, and current remediation  
567 technologies, *Environ. Int.*, 2014, **71**, 118-138.
- 568 3. S. B. Ge, N. L. Ma, S. C. Jiang, Y. S. Ok, S. S. Lam, C. Li, S. Q. Shi, X. Nie, Y. Qiu, D. L. Li, Q. D. Wu,  
569 D. C. W. Tsang, W. X. Peng and C. Sonne, Processed Bamboo as a Novel Formaldehyde-Free  
570 High-Performance Furniture Biocomposite, *ACS Appl. Mater. Interfaces*, 2020, **12**, 30824-30832.
- 571 4. H. K. Yuan, J. Ren, X. H. Ma and Z. L. Xu, Dehydration of ethyl acetate aqueous solution by  
572 pervaporation using PVA/PAN hollow fiber composite membrane, *Desalination*, 2011, **280**,  
573 252-258.
- 574 5. P. I. Beamer, C. E. Luik, L. Abrell, S. Campos, M. E. Martinez and A. E. Saez, Concentration of  
575 Trichloroethylene in Breast Milk and Household Water from Nogales, Arizona, *Environ. Sci.*  
576 *Technol.*, 2012, **46**, 9055-9061.
- 577 6. R. Baran, Kaminska, II, A. Srebrowata and S. Dzwigaj, Selective hydrodechlorination of 1,2-  
578 dichloroethane on NiSIBEA zeolite catalyst: Influence of the preparation procedure on a high  
579 dispersion of Ni centers, *Microporous Mesoporous Mat.*, 2013, **169**, 120-127.
- 580 7. Y. C. Chien, Variations in amounts and potential sources of volatile organic chemicals in new  
581 cars, *Sci. Total Environ.*, 2007, **382**, 228-239.
- 582 8. M. R. Gwinn, D. O. Johns, T. F. Bateson and K. Z. Guyton, A review of the genotoxicity of 1,2-  
583 dichloroethane (EDC), *Mutation Research-Reviews in Mutation Research*, 2011, **727**, 42-53.
- 584 9. B. C. McDonald, J. A. de Gouw, J. B. Gilman, S. H. Jathar, A. Akherati, C. D. Cappa, J. L. Jimenez,  
585 J. Lee-Taylor, P. L. Hayes, S. A. McKeen, Y. Y. Cui, S.-W. Kim, D. R. Gentner, G. Isaacman-VanWertz,  
586 A. H. Goldstein, R. A. Harley, G. J. Frost, J. M. Roberts, T. B. Ryerson and M. Trainer, Volatile  
587 chemical products emerging as largest petrochemical source of urban organic emissions,  
588 *Science*, 2018, **359**, 760-764.
- 589 10. Z. M. Zhong, Q. E. Sha, J. Y. Zheng, Z. B. Yuan, Z. J. Gao, J. M. Ou, Z. Y. Zheng, C. Li and Z. J. Huang,  
590 Sector-based VOCs emission factors and source profiles for the surface coating industry in the  
591 Pearl River Delta region of China, *Sci. Total Environ.*, 2017, **583**, 19-28.
- 592 11. J. L. Jiang, X. S. Ding, A. Tasoglou, H. Huber, A. D. Shah, N. Jung and B. E. Boor, Real-Time  
593 Measurements of Botanical Disinfectant Emissions, Transformations, and Multiphase  
594 Inhalation Exposures in Buildings, *Environ. Sci. Technol. Lett.*, 2021, **8**, 558-566.
- 595 12. X. H. Zhang, Q. L. Liu, Y. Xiong, A. M. Zhu, Y. Chen and Q. G. Zhang, Pervaporation dehydration  
596 of ethyl acetate/ethanol/water azeotrope using chitosan/poly (vinyl pyrrolidone) blend  
597 membranes, *J. Membr. Sci.*, 2009, **327**, 274-280.

- 598 13. R. J. Keith, J. L. Fetterman, O. A. Orimoloye, Z. Dardari, P. K. Lorkiewicz, N. M. Hamburg, A. P.  
599 DeFilippis, M. J. Blaha and A. Bhatnagar, Characterization of Volatile Organic Compound  
600 Metabolites in Cigarette Smokers, Electronic Nicotine Device Users, Dual Users, and Nonusers  
601 of Tobacco, *Nicotine Tob. Res.*, 2020, **22**, 264-272.
- 602 14. Z. Zhang, Z. Jiang and W. Shangguan, Low-temperature catalysis for VOCs removal in  
603 technology and application: A state-of-the-art review, *Catalysis Today*, 2016, **264**, 270-278.
- 604 15. C. He, J. Cheng, X. Zhang, M. Douthwaite, S. Pattisson and Z. Hao, Recent Advances in the  
605 Catalytic Oxidation of Volatile Organic Compounds: A Review Based on Pollutant Sorts and  
606 Sources, *Chem. Rev.*, 2019, **119**, 4471-4568.
- 607 16. U. Poschl and M. Shiraiwa, Multiphase Chemistry at the Atmosphere-Biosphere Interface  
608 Influencing Climate and Public Health in the Anthropocene, *Chem. Rev.*, 2015, **115**, 4440-4475.
- 609 17. C. P. Weisel, Assessing exposure to air toxics relative to asthma, *Environmental Health  
610 Perspectives*, 2002, **110**, 527-537.
- 611 18. S. Weichenthal, R. Kulka, P. Belisle, L. Joseph, A. Dubeau, C. Martin, D. Wang and R. Dales,  
612 Personal exposure to specific volatile organic compounds and acute changes in lung function  
613 and heart rate variability among urban cyclists, *Environ. Res.*, 2012, **118**, 118-123.
- 614 19. R. Xiao, J. Mo, Y. Zhang and D. Gao, An in-situ thermally regenerated air purifier for indoor  
615 formaldehyde removal, *Indoor Air*, 2018, **28**, 266-275.
- 616 20. K. Rumchev, J. Spickett, M. Bulsara, M. Phillips and S. Stick, Association of domestic exposure  
617 to volatile organic compounds with asthma in young children, *Thorax*, 2004, **59**, 746-751.
- 618 21. X. Zhang, B. Gao, A. E. Creamer, C. Cao and Y. Li, Adsorption of VOCs onto engineered carbon  
619 materials: A review, *Journal of Hazardous Materials*, 2017, **338**, 102-123.
- 620 22. W. X. Zou, B. Gao, Y. S. Ok and L. Dong, Integrated adsorption and photocatalytic degradation  
621 of volatile organic compounds (VOCs) using carbon-based nanocomposites: A critical review,  
622 *Chemosphere*, 2019, **218**, 845-859.
- 623 23. U. I. Gaya and A. H. Abdullah, Heterogeneous photocatalytic degradation of organic  
624 contaminants over titanium dioxide: A review of fundamentals, progress and problems, *J.  
625 Photochem. Photobiol. C-Photochem. Rev.*, 2008, **9**, 1-12.
- 626 24. M. Tahir, S. Tasleem and B. Tahir, Recent development in band engineering of binary  
627 semiconductor materials for solar driven photocatalytic hydrogen production, *Int. J. Hydrog.  
628 Energy*, 2020, **45**, 15985-16038.
- 629 25. T. K. Tseng, Y. S. Lin, Y. J. Chen and H. Chu, A Review of Photocatalysts Prepared by Sol-Gel  
630 Method for VOCs Removal, *Int. J. Mol. Sci.*, 2010, **11**, 2336-2361.
- 631 26. M. Adeel, N. Shakoor, T. Hussain, I. Azeem, P. F. Zhou, P. Zhang, Y. Hao, J. Rinklebe and Y. K. Rui,  
632 Bio-interaction of nano and bulk lanthanum and ytterbium oxides in soil system: Biochemical,  
633 genetic, and histopathological effects on *Eisenia fetida*, *Journal of Hazardous Materials*, 2021,  
634 **415**.
- 635 27. R. K. Huang, C. Y. Cao, J. Liu, L. R. Zheng, Q. H. Zhang, L. Gu, L. Jiang and W. G. Song, Integration  
636 of Metal Single Atoms on Hierarchical Porous Nitrogen-Doped Carbon for Highly Efficient  
637 Hydrogenation of Large-Sized Molecules in the Pharmaceutical Industry, *ACS Appl. Mater.  
638 Interfaces*, 2020, **12**, 17651-17658.
- 639 28. Y. L. Zhao, Y. L. Song, W. G. Song, W. Liang, X. Y. Jiang, Z. Y. Tang, H. X. Xu, Z. X. Wei, Y. Q. Liu, M.  
640 H. Liu, L. Jiang, X. H. Bao, L. J. Wan and C. L. Bai, Progress of nanoscience in China, *Frontiers of  
641 Physics*, 2014, **9**, 257-288.
- 642 29. M. M. Rui, C. X. Ma, J. C. White, Y. Hao, Y. Y. Wang, X. L. Tang, J. Yang, F. P. Jiang, A. Ali, Y. K. Rui,  
643 W. D. Cao, G. C. Chen and B. S. Xing, Metal oxide nanoparticles alter peanut (*Arachis hypogaea*  
644 L.) physiological response and reduce nutritional quality: a life cycle study, *Environ. Sci.-Nano*,  
645 2018, **5**, 2088-2102.
- 646 30. C. Santhosh, V. Velmurugan, G. Jacob, S. K. Jeong, A. N. Grace and A. Bhatnagar, Role of  
647 nanomaterials in water treatment applications: A review, *Chemical Engineering Journal*, 2016,  
648 **306**, 1116-1137.
- 649 31. D. S. Selishchev, T. N. Filippov, M. N. Lyulyukin and D. V. Kozlov, Uranyl-modified TiO<sub>2</sub> for  
650 complete photocatalytic oxidation of volatile organic compounds under UV and visible light,  
651 *Chemical Engineering Journal*, 2019, **370**, 1440-1449.
- 652 32. X. Liu, J. Iocozzia, Y. Wang, X. Cui, Y. Chen, S. Zhao, Z. Li and Z. Lin, Noble metal-metal oxide  
653 nanohybrids with tailored nanostructures for efficient solar energy conversion, photocatalysis  
654 and environmental remediation, *Energy & Environmental Science*, 2017, **10**, 402-434.



- 655 33. Q. K. Shen, C. Y. Cao, R. K. Huang, L. Zhu, X. Zhou, Q. H. Zhang, L. Gu and W. G. Song, Single  
656 Chromium Atoms Supported on Titanium Dioxide Nanoparticles for Synergic Catalytic Methane  
657 Conversion under Mild Conditions, *Angew. Chem.-Int. Edit.*, 2020, **59**, 1216-1219.
- 658 34. A. Suligoj, U. L. Stanger, A. Ristic, M. Mazaj, D. Verhovsek and N. N. Tusar, TiO<sub>2</sub>-SiO<sub>2</sub> films from  
659 organic-free colloidal TiO<sub>2</sub> anatase nanoparticles as photocatalyst for removal of volatile  
660 organic compounds from indoor air, *Applied Catalysis B-Environmental*, 2016, **184**, 119-131.
- 661 35. S. Suarez, I. Jansson, B. Ohtani and B. Sanchez, From titania nanoparticles to decahedral  
662 anatase particles: Photocatalytic activity of TiO<sub>2</sub>/zeolite hybrids for VOCs oxidation, *Catalysis  
663 Today*, 2019, **326**, 2-7.
- 664 36. C. Karthikeyan, P. Arunachalam, K. Ramachandran, A. M. Al-Mayouf and S. Karuppuchamy,  
665 Recent advances in semiconductor metal oxides with enhanced methods for solar  
666 photocatalytic applications, *J. Alloy. Compd.*, 2020, **828**, 15.
- 667 37. Z. Shayegan, C. S. Lee and F. Haghghat, TiO<sub>2</sub> photocatalyst for removal of volatile organic  
668 compounds in gas phase - A review, *Chemical Engineering Journal*, 2018, **334**, 2408-2439.
- 669 38. Z. J. Zhu, Q. Zhang, X. Xiao, F. Q. Sun, X. X. Zuo and J. M. Nan, Dual-iodine-doped BiOIO<sub>3</sub>: Bulk  
670 and surface co-modification for enhanced visible-light photocatalytic removal of bisphenol AF,  
671 *Chemical Engineering Journal*, 2021, **404**, 13.
- 672 39. S. G. Kumar and R. Kavitha, Lanthanide ions doped ZnO based photocatalysts, *Sep. Purif.  
673 Technol.*, 2021, **274**, 33.
- 674 40. K. Li, S. Zhang, Y. Li, J. Fan and K. Lv, MXenes as noble-metal-alternative co-catalysts in  
675 photocatalysis, *Chinese Journal of Catalysis*, 2021, **42**, 3-14.
- 676 41. M. Malakootian, A. Nasiri and M. A. Gharaghani, Photocatalytic degradation of ciprofloxacin  
677 antibiotic by TiO<sub>2</sub> nanoparticles immobilized on a glass plate, *Chemical Engineering  
678 Communications*, 2020, **207**, 56-72.
- 679 42. H. Zangeneh, A. A. L. Zinatizadeh, M. Habibi, M. Akia and M. H. Isa, Photocatalytic oxidation of  
680 organic dyes and pollutants in wastewater using different modified titanium dioxides: A  
681 comparative review, *J. Ind. Eng. Chem.*, 2015, **26**, 1-36.
- 682 43. Q. Guo, C. Y. Zhou, Z. B. Ma and X. M. Yang, Fundamentals of TiO<sub>2</sub> Photocatalysis: Concepts,  
683 Mechanisms, and Challenges, *Adv. Mater.*, 2019, **31**, 26.
- 684 44. H. Yi, L. Qin, D. L. Huang, G. M. Zeng, C. Lai, X. G. Liu, B. S. Li, H. Wang, C. Y. Zhou, F. L. Huang,  
685 S. Y. Liu and X. Y. Guo, Nano-structured bismuth tungstate with controlled morphology:  
686 Fabrication, modification, environmental application and mechanism insight, *Chemical  
687 Engineering Journal*, 2019, **358**, 480-496.
- 688 45. C. P. Xu, P. R. Anusuyadevi, C. Aymonier, R. Luque and S. Marre, Nanostructured materials for  
689 photocatalysis, *Chem. Soc. Rev.*, 2019, **48**, 3868-3902.
- 690 46. B. S. Li, C. Lai, G. M. Zeng, D. L. Huang, L. Qin, M. M. Zhang, M. Cheng, X. G. Liu, H. Yi, C. Y. Zhou,  
691 F. L. Huang, S. Y. Liu and Y. K. Fu, Black Phosphorus, a Rising Star 2D Nanomaterial in the Post-  
692 Graphene Era: Synthesis, Properties, Modifications, and Photocatalysis Applications, *Small*,  
693 2019, **15**.
- 694 47. G. Liu, W. Xi, X. You, Y. Zhi, C. Li and Iop, Sanya, PEOPLES R CHINA, 2018.
- 695 48. U. B. Celebi and N. Vardar, Investigation of VOC emissions from indoor and outdoor painting  
696 processes in shipyards, *Atmospheric Environment*, 2008, **42**, 5685-5695.
- 697 49. H. Wang, L. Nie, J. Li, Y. Wang, G. Wang, J. Wang and Z. Hao, Characterization and assessment  
698 of volatile organic compounds (VOCs) emissions from typical industries, *Chinese Science  
699 Bulletin*, 2013, **58**, 724-730.
- 700 50. K. Yang, C. Wang, S. Xue, W. Li, J. Liu and L. Li, The identification, health risks and olfactory  
701 effects assessment of VOCs released from the wastewater storage tank in a pesticide plant,  
702 *Ecotoxicology and Environmental Safety*, 2019, **184**.
- 703 51. S. M. T. Sendesi, Y. Noh, M. Nuruddin, B. E. Boor, J. A. Howarter, J. P. Youngblood, C. T. Jafvert  
704 and A. J. Whelton, An emerging mobile air pollution source: outdoor plastic liner  
705 manufacturing sites discharge VOCs into urban and rural areas, *Environmental Science-  
706 Processes & Impacts*, 2020, **22**, 1828-1841.
- 707 52. Y. Liu, F. Han, W. Liu, X. Cui, X. Luan and Z. Cui, Process-based volatile organic compound  
708 emission inventory establishment method for the petroleum refining industry, *J. Clean Prod.*,  
709 2020, **263**.
- 710 53. X. Zhang, D. Wang, Y. Liu, Y. Cui, Z. Xue, Z. Gao and J. Du, Characteristics and ozone formation  
711 potential of volatile organic compounds in emissions from a typical Chinese coking plant,

- 712 *Journal of Environmental Sciences*, 2020, **95**, 183-189.
- 713 54. Q. Li, G. Su, C. Li, M. Wang, L. Tan, L. Gao, M. Wu and Q. Wang, Emission profiles, ozone  
714 formation potential and health-risk assessment of volatile organic compounds in rubber  
715 footwear industries in China, *Journal of Hazardous Materials*, 2019, **375**, 52-60.
- 716 55. C. T. Chang and K. L. Lin, Assessment of the strategies for reducing VOCs emission from  
717 polyurea-formaldehyde resin synthetic fiber leather industry in Taiwan, *Resources  
718 Conservation and Recycling*, 2006, **46**, 321-334.
- 719 56. N. Cheng, D. Jing, C. Zhang, Z. Chen, W. Li, S. Li and Q. Wang, Process-based VOCs source  
720 profiles and contributions to ozone formation and carcinogenic risk in a typical chemical  
721 synthesis pharmaceutical industry in China, *Sci. Total Environ.*, 2021, **752**.
- 722 57. H.-H. Yang, S. K. Gupta and N. B. Dhital, Emission factor, relative ozone formation potential and  
723 relative carcinogenic risk assessment of VOCs emitted from manufacturing industries,  
724 *Sustainable Environment Research*, 2020, **30**.
- 725 58. H. H. Chen, C. E. Nanayakkara and V. H. Grassian, Titanium Dioxide Photocatalysis in  
726 Atmospheric Chemistry, *Chem. Rev.*, 2012, **112**, 5919-5948.
- 727 59. Q. Guo, C. Zhou, Z. Ma, Z. Ren, H. Fan and X. Yang, Elementary photocatalytic chemistry on  
728 TiO<sub>2</sub> surfaces, *Chem. Soc. Rev.*, 2016, **45**, 3701-3730.
- 729 60. M. A. Henderson, A surface science perspective on TiO<sub>2</sub> photocatalysis, *Surf. Sci. Rep.*, 2011,  
730 **66**, 185-297.
- 731 61. S. H. Zhan, Y. Yang, X. C. Gao, H. B. Yu, S. S. Yang, D. D. Zhu and Y. Li, Rapid degradation of toxic  
732 toluene using novel mesoporous SiO<sub>2</sub> doped TiO<sub>2</sub> nanofibers, *Catalysis Today*, 2014, **225**, 10-  
733 17.
- 734 62. A. H. Mamaghani, F. Haghghat and C. S. Lee, Photocatalytic oxidation technology for indoor  
735 environment air purification: The state-of-the-art, *Applied Catalysis B-Environmental*, 2017,  
736 **203**, 247-269.
- 737 63. A. Bazyari, A. A. Khodadadi, A. H. Mamaghani, J. Beheshtian, L. T. Thompson and Y. Mortazavi,  
738 Microporous titania-silica nanocomposite catalyst-adsorbent for ultra-deep oxidative  
739 desulfurization, *Applied Catalysis B-Environmental*, 2016, **180**, 65-77.
- 740 64. V. Puddu, H. Choi, D. D. Dionysiou and G. L. Puma, TiO<sub>2</sub> photocatalyst for indoor air remediation:  
741 Influence of crystallinity, crystal phase, and UV radiation intensity on trichloroethylene  
742 degradation, *Applied Catalysis B-Environmental*, 2010, **94**, 211-218.
- 743 65. Z. Long, Q. Li, T. Wei, G. Zhang and Z. Ren, Historical development and prospects of  
744 photocatalysts for pollutant removal in water, *Journal of Hazardous Materials*, 2020, **395**.
- 745 66. S. Wang, Q. Sun, W. Chen, Y. Q. Tang, B. Aguila, Y. X. Pan, A. M. Zheng, Z. Y. Yang, L. Wojtas, S.  
746 Q. Ma and F. S. Xiao, Programming Covalent Organic Frameworks for Photocatalysis:  
747 Investigation of Chemical and Structural Variations, *Matter*, 2020, **2**, 416-427.
- 748 67. R. O. Da Silva, R. H. Goncalves, D. G. Stroppa, A. J. Ramirez and E. R. Leite, Synthesis of  
749 recrystallized anatase TiO<sub>2</sub> mesocrystals with Wulff shape assisted by oriented attachment,  
750 *Nanoscale*, 2011, **3**, 1910-1916.
- 751 68. P. Pleskunov, T. Kosutova, M. Vaidulych, D. Nikitin, Z. Krtous, S. Ali-Ogly, K. Kishenina, R.  
752 Tafiichuk, H. Biederman, I. Gordeev, J. Drewes, I. Barg, F. Faupel, M. Cieslar, R. Yatskiv, Y. Pihosh,  
753 V. Nandal, K. Seki, K. Domen and A. Choukourov, The sputter-based synthesis of tantalum  
754 oxynitride nanoparticles with architecture and bandgap controlled by design, *Appl. Surf. Sci.*,  
755 2021, **559**.
- 756 69. T. Katsuki, Z. N. Zahran, K. Tanaka, T. Eo, E. A. Mohamed, Y. Tsubonouchi, M. R. Berber and M.  
757 Yagi, Facile Fabrication of a Highly Crystalline and Well-Interconnected Hematite Nanoparticle  
758 Photoanode for Efficient Visible-Light-Driven Water Oxidation, *ACS Appl. Mater. Interfaces*,  
759 2021, **13**, 39282-39290.
- 760 70. Q. Li, J. Wang, Y. Z. Zhang, L. Ricardez-Sandoval, G. Y. Bai and X. W. Lan, Structural and  
761 Morphological Engineering of Benzothiadiazole-Based Covalent Organic Frameworks for  
762 Visible Light-Driven Oxidative Coupling of Amines, *ACS Appl. Mater. Interfaces*, 2021, **13**,  
763 39291-39303.
- 764 71. I. S. Curtis, R. J. Wills and M. Dasog, Photocatalytic hydrogen generation using mesoporous  
765 silicon nanoparticles: influence of magnesiothermic reduction conditions and nanoparticle  
766 aging on the catalytic activity, *Nanoscale*, 2021, **13**, 2685-2692.
- 767 72. Q. L. Li, T. Song, Y. P. Zhang, Q. Wang and Y. Yang, Boosting Photocatalytic Activity and Stability  
768 of Lead-Free Cs<sub>3</sub>Bi<sub>2</sub>Br<sub>9</sub> Perovskite Nanocrystals via In Situ Growth on Monolayer 2D Ti<sub>3</sub>C<sub>2</sub>T<sub>x</sub>

- 769 MXene for C-H Bond Oxidation, *ACS Appl. Mater. Interfaces*, 2021, **13**, 27323-27333.
- 770 73. Y. H. Zhang, G. D. Shen, C. H. Sheng, F. Zhang and W. Fan, The effect of piezo-photocatalysis on  
771 enhancing the charge carrier separation in BaTiO<sub>3</sub>/KNbO<sub>3</sub> heterostructure photocatalyst, *Appl.*  
772 *Surf. Sci.*, 2021, **562**, 12.
- 773 74. A. Alonso-Tellez, R. Masson, D. Robert, N. Keller and V. Keller, Comparison of Hombikat UV100  
774 and P25 TiO<sub>2</sub> performance in gas-phase photocatalytic oxidation reactions, *Journal of*  
775 *Photochemistry and Photobiology a-Chemistry*, 2012, **250**, 58-65.
- 776 75. K. Nakata and A. Fujishima, TiO<sub>2</sub> photocatalysis: Design and applications, *J. Photochem.*  
777 *Photobiol. C-Photochem. Rev.*, 2012, **13**, 169-189.
- 778 76. M. Xiao, Z. L. Wang, M. Q. Lyu, B. Luo, S. C. Wang, G. Liu, H. M. Cheng and L. Z. Wang, Hollow  
779 Nanostructures for Photocatalysis: Advantages and Challenges, *Adv. Mater.*, 2019, **31**, 23.
- 780 77. M. Hajaghazadeh, V. Vaiano, D. Sannino, H. Kakooei, R. Sotudeh-Gharebagh and P. Ciambelli,  
781 Heterogeneous photocatalytic oxidation of methyl ethyl ketone under UV-A light in an LED-  
782 fluidized bed reactor, *Catalysis Today*, 2014, **230**, 79-84.
- 783 78. J. Taranto, D. Frochot and P. Pichat, Photocatalytic Treatment of Air: Comparison of Various  
784 TiO<sub>2</sub>, Coating Methods, and Supports Using Methanol or n-Octane as Test Pollutant, *Industrial*  
785 *& Engineering Chemistry Research*, 2009, **48**, 6229-6236.
- 786 79. Y. T. Liu, Q. P. Zhang, M. Xu, H. Yuan, Y. Chen, J. X. Zhang, K. Y. Luo, J. Q. Zhang and B. A. You,  
787 Novel and efficient synthesis of Ag-ZnO nanoparticles for the sunlight-induced photocatalytic  
788 degradation, *Appl. Surf. Sci.*, 2019, **476**, 632-640.
- 789 80. M. Rajca, NOM (HA and FA) Reduction in Water Using Nano Titanium Dioxide Photocatalysts  
790 (P25 and P90) and Membranes, *Catalysts*, 2020, **10**, 13.
- 791 81. N. Chen, Q. N. Gong, F. Wang, J. Ren, R. X. Wang and W. Z. Jiao, N-doped porous carbon-  
792 stabilized Pt in hollow nano-TiO<sub>2</sub> with enhanced photocatalytic activity, *Int. J. Hydrog. Energy*,  
793 2020, **45**, 24779-24791.
- 794 82. W.-H. Li, K. Ding, H.-R. Tian, M.-S. Yao, B. Nath, W.-H. Deng, Y. Wang and G. Xu, Conductive  
795 Metal-Organic Framework Nanowire Array Electrodes for High-Performance Solid-State  
796 Supercapacitors, *Advanced Functional Materials*, 2017, **27**.
- 797 83. S. Wang, C. M. McQuirk, A. d'Aquino, J. A. Mason and C. A. Mirkin, Metal-Organic Framework  
798 Nanoparticles, *Adv. Mater.*, 2018, **30**.
- 799 84. Y. Zhang, X. Feng, S. Yuan, J. Zhou and B. Wang, Challenges and recent advances in MOF-  
800 polymer composite membranes for gas separation, *Inorg. Chem. Front.*, 2016, **3**, 896-909.
- 801 85. Y. B. Dou, J. Zhou, A. Zhou, J. R. Li and Z. R. Nie, Visible-light responsive MOF encapsulation of  
802 noble-metal-sensitized semiconductors for high-performance photoelectrochemical water  
803 splitting, *J. Mater. Chem. A*, 2017, **5**, 19491-19498.
- 804 86. W. L. Xue, L. Wang, Y. K. Li, H. Chen, K. X. Fu, F. Zhang, T. He, Y. H. Deng, J. R. Li and C. Q. Wan,  
805 Reticular Chemistry for Ionic Liquid-Functionalized Metal-Organic Frameworks with High  
806 Selectivity for CO<sub>2</sub>, *Acs Sustainable Chemistry & Engineering*, 2020, **8**, 18558-18567.
- 807 87. L.-H. Xie, X.-M. Liu, T. He and J.-R. Li, Metal-Organic Frameworks for the Capture of Trace  
808 Aromatic Volatile Organic Compounds, *Chem*, 2018, **4**, 1911-1927.
- 809 88. J. Y. Wu, C. L. Tang, W. Y. Zhang, X. X. Ma, S. W. Qu, K. X. Chen, T. Hao and S. Chiang, Lab on  
810 optical fiber: surface nano-functionalization for real-time monitoring of VOC  
811 adsorption/desorption in metal-organic frameworks, *Nanophotonics*, 2021, **10**, 2705-2716.
- 812 89. M. J. Wang, Z. R. Shen, X. D. Zhao, F. P. Duanmu, H. J. Yu and H. M. Ji, Rational shape control of  
813 porous Co<sub>3</sub>O<sub>4</sub> assemblies derived from MOF and their structural effects on n-butanol sensing,  
814 *Journal of Hazardous Materials*, 2019, **371**, 352-361.
- 815 90. Q. Yu, R. R. Jin, L. P. Zhao, T. S. Wang, F. M. Liu, X. Yan, C. G. Wang, P. Sun and G. Y. Lu, MOF-  
816 Derived Mesoporous and Hierarchical Hollow-Structured In<sub>2</sub>O<sub>3</sub>-NiO Composites for Enhanced  
817 Triethylamine Sensing, *Acs Sensors*, 2021, **6**, 3451-3461.
- 818 91. D. A. Giannakoudakis, A. Qayyum, D. Lomot, M. O. Besenhard, D. Lisovytskiy, T. J. Bandoz and  
819 J. C. Colmenares, Boosting the Photoactivity of Grafted Titania: Ultrasound-Driven Synthesis of  
820 a Multi-Phase Heterogeneous Nano-Architected Photocatalyst, *Advanced Functional Materials*,  
821 2021, **31**.
- 822 92. H. Wei, W. A. McMaster, J. Z. Y. Tan, D. H. Chen and R. A. Caruso, Tricomponent  
823 brookite/anatase TiO<sub>2</sub>/g-C<sub>3</sub>N<sub>4</sub> heterojunction in mesoporous hollow microspheres for  
824 enhanced visible-light photocatalysis, *J. Mater. Chem. A*, 2018, **6**, 7236-7245.
- 825 93. M. Q. Hu, Y. Cao, Z. Z. Li, S. L. Yang and Z. P. Xing, Ti<sup>3+</sup> self-doped mesoporous black TiO<sub>2</sub>/SiO<sub>2</sub>

- 826 nanocomposite as remarkable visible light photocatalyst, *Appl. Surf. Sci.*, 2017, **426**, 734-744.
- 827 94. N. Quici, M. L. Vera, H. Choi, G. L. Puma, D. D. Dionysiou, M. I. Litter and H. Destailats, Effect of  
828 key parameters on the photocatalytic oxidation of toluene at low concentrations in air under  
829 254+185 nm UV irradiation, *Applied Catalysis B-Environmental*, 2010, **95**, 312-319.
- 830 95. R. Singh, R. Bapat, L. J. Qin, H. Feng and V. Polshettiwar, Atomic Layer Deposited (ALD) TiO<sub>2</sub> on  
831 Fibrous Nano-Silica (KCC-1) for Photocatalysis: Nanoparticle Formation and Size Quantization  
832 Effect, *Acs Catalysis*, 2016, **6**, 2770-2784.
- 833 96. X. N. Wang, R. Long, D. Liu, D. Yang, C. M. Wang and Y. J. Xiong, Enhanced full-spectrum water  
834 splitting by confining plasmonic Au nanoparticles in N-doped TiO<sub>2</sub> bowl nanoarrays, *Nano  
835 Energy*, 2016, **24**, 87-93.
- 836 97. M. V. Roldan, P. de Ona, Y. Castro, A. Duran, P. Faccendini, C. Lagier, R. Grau and N. S. Pellegrini,  
837 Photocatalytic and biocidal activities of novel coating systems of mesoporous and dense TiO<sub>2</sub>-  
838 anatase containing silver nanoparticles, *Materials Science & Engineering C-Materials for  
839 Biological Applications*, 2014, **43**, 630-640.
- 840 98. Z. Zhang, G. H. Wang, W. B. Li, L. D. Zhang, B. W. Guo, L. Ding and X. C. Li, Photocatalytic Activity  
841 of Magnetic Nano-beta-FeOOH/Fe<sub>3</sub>O<sub>4</sub>/Biochar Composites for the Enhanced Degradation of  
842 Methyl Orange Under Visible Light, *Nanomaterials*, 2021, **11**.
- 843 99. J. J. Zhang, Y. X. Li, L. Li, W. L. Li and C. F. Yang, Dual Functional N-Doped TiO<sub>2</sub>-Carbon Composite  
844 Fibers for Efficient Removal of Water Pollutants, *Acs Sustainable Chemistry & Engineering*, 2018,  
845 **6**, 12893-12905.
- 846 100. S. Shamaila, A. K. L. Sajjad, A. Quart ul, S. Shaheen, A. Iqbal, S. Noor, G. Sughra and U. Ali, A  
847 cost effective and eco-friendly green route for fabrication of efficient graphene nanosheets  
848 photocatalyst, *J. Environ. Chem. Eng.*, 2017, **5**, 5770-5776.
- 849 101. S. Noor, S. Sajjad, S. A. K. Leghari, C. Flox, T. Kallio, E. I. Kauppinen and S. Ahmad, Electronic  
850 transitions of SWCNTs in comparison to GO on Mn<sub>3</sub>O<sub>4</sub>/TiO<sub>2</sub> nanocomposites for hydrogen  
851 energy generation and solar photocatalysis, *New Journal of Chemistry*, 2021, **45**, 2431-2442.
- 852 102. Z. Yousaf, S. Sajjad, S. A. K. Leghari, M. Mehboob, A. Kanwal and B. Uzair, Interfacial charge  
853 transfer via 2D-NiO and 2D-graphene nanosheets combination for significant visible  
854 photocatalysis, *Journal of Solid State Chemistry*, 2020, **291**.
- 855 103. S. Noor, S. Sajjad, S. A. K. Leghari and M. C. Long, Energy harvesting for electrochemical OER  
856 and solar photocatalysis via dual functional GO/TiO<sub>2</sub>-NiO nanocomposite, *J. Clean Prod.*, 2020,  
857 **277**.
- 858 104. F. Fresno, M. D. Hernandez-Alonso, D. Tudela, J. M. Coronado and J. Soria, Photocatalytic  
859 degradation of toluene over doped and coupled (Ti,M)O<sub>2</sub> (M = Sn or Zr) nanocrystalline oxides:  
860 Influence of the heteroatom distribution on deactivation, *Applied Catalysis B-Environmental*,  
861 2008, **84**, 598-606.
- 862 105. M. Takeuchi, J. Deguchi, S. Sakai and M. Anpo, Effect of H<sub>2</sub>O vapor addition on the  
863 photocatalytic oxidation of ethanol, acetaldehyde and acetic acid in the gas phase on TiO<sub>2</sub>  
864 semiconductor powders, *Applied Catalysis B-Environmental*, 2010, **96**, 218-223.
- 865 106. M. J. Munoz-Batista, A. Kubacka, M. Natividad Gomez-Cerezo, D. Tudela and M. Fernandez-  
866 Garcia, Sunlight-driven toluene photo-elimination using CeO<sub>2</sub>-TiO<sub>2</sub> composite systems: A  
867 kinetic study, *Applied Catalysis B-Environmental*, 2013, **140**, 626-635.
- 868 107. N. Bouazza, M. A. Lillo-Rodenas and A. Linares-Solano, Photocatalytic activity of TiO<sub>2</sub>-based  
869 materials for the oxidation of propene and benzene at low concentration in presence of  
870 humidity, *Applied Catalysis B-Environmental*, 2008, **84**, 691-698.
- 871 108. H. Einaga, S. Futamura and T. Ibusuki, Heterogeneous photocatalytic oxidation of benzene,  
872 toluene, cyclohexene and cyclohexane in humidified air: comparison of decomposition  
873 behavior on photoirradiated TiO<sub>2</sub> catalyst, *Applied Catalysis B-Environmental*, 2002, **38**, 215-  
874 225.
- 875 109. T. Guo, Z. Bai, C. Wu and T. Zhu, Influence of relative humidity on the photocatalytic oxidation  
876 (PCO) of toluene by TiO<sub>2</sub> loaded on activated carbon fibers: PCO rate and intermediates  
877 accumulation, *Applied Catalysis B-Environmental*, 2008, **79**, 171-178.
- 878 110. G. Vincent, P. M. Marquaire and O. Zahraa, Photocatalytic degradation of gaseous 1-propanol  
879 using an annular reactor: Kinetic modelling and pathways, *Journal of Hazardous Materials*,  
880 2009, **161**, 1173-1181.
- 881 111. R. A. R. Monteiro, A. M. T. Silva, J. R. M. Angelo, G. V. Silva, A. M. Mendes, R. A. R. Boaventura  
882 and V. J. P. Vilar, Photocatalytic oxidation of gaseous perchloroethylene over TiO<sub>2</sub> based paint,

- 883 *Journal of Photochemistry and Photobiology a-Chemistry*, 2015, **311**, 41-52.
- 884 112. Y. Huang, H. Hu, S. Wang, M.-S. Balogun, H. Ji and Y. Tong, Low concentration nitric acid facilitate  
885 rapid electron-hole separation in vacancy-rich bismuth oxyiodide for photo-thermo-synergistic  
886 oxidation of formaldehyde, *Applied Catalysis B-Environmental*, 2017, **218**, 700-708.
- 887 113. Y. Tao, C.-Y. Wu and D. W. Mazyck, Removal of methanol from pulp and paper mills using  
888 combined activated carbon adsorption and photocatalytic regeneration, *Chemosphere*, 2006,  
889 **65**, 35-42.
- 890 114. B. M. da Costa Filho, A. L. P. Araujo, G. V. Silva, R. A. R. Boaventura, M. M. Dias, J. C. B. Lopes  
891 and V. J. P. Vilar, Intensification of heterogeneous TiO<sub>2</sub> photocatalysis using an innovative  
892 micro-meso-structured-photoreactor for n-decane oxidation at gas phase, *Chemical  
893 Engineering Journal*, 2017, **310**, 331-341.
- 894 115. Z. Han, V.-W. Chang, X. Wang, T.-T. Lim and L. Hildemann, Experimental study on visible-light  
895 induced photocatalytic oxidation of gaseous formaldehyde by polyester fiber supported  
896 photocatalysts, *Chemical Engineering Journal*, 2013, **218**, 9-18.
- 897 116. M. Hussain, N. Russo and G. Saracco, Photocatalytic abatement of VOCs by novel optimized  
898 TiO<sub>2</sub> nanoparticles, *Chemical Engineering Journal*, 2011, **166**, 138-149.
- 899 117. F. Moulis and J. Krysa, Photocatalytic degradation of several VOCs (n-hexane, n-butyl acetate  
900 and toluene) on TiO<sub>2</sub> layer in a closed-loop reactor, *Catalysis Today*, 2013, **209**, 153-158.
- 901 118. L. Zhong, F. Haghighat, C.-S. Lee and N. Lakdawala, Performance of ultraviolet photocatalytic  
902 oxidation for indoor air applications: Systematic experimental evaluation, *Journal of Hazardous  
903 Materials*, 2013, **261**, 130-138.
- 904 119. Y. X. Deng, Developing a Langmuir-type excitation equilibrium equation to describe the effect  
905 of light intensity on the kinetics of the photocatalytic oxidation, *Chemical Engineering Journal*,  
906 2018, **337**, 220-227.
- 907 120. L. Pinho, M. Rojas and M. J. Mosquera, Ag-SiO<sub>2</sub>-TiO<sub>2</sub> nanocomposite coatings with enhanced  
908 photoactivity for self-cleaning application on building materials, *Applied Catalysis B-  
909 Environmental*, 2015, **178**, 144-154.
- 910 121. S. Sun, J. Ding, J. Bao, C. Gao, Z. Qi, X. Yang, B. He and C. Li, Photocatalytic degradation of  
911 gaseous toluene on Fe-TiO<sub>2</sub> under visible light irradiation: A study on the structure, activity  
912 and deactivation mechanism, *Appl. Surf. Sci.*, 2012, **258**, 5031-5037.
- 913 122. R. Dagherir, P. Drogui and D. Robert, Modified TiO<sub>2</sub> For Environmental Photocatalytic  
914 Applications: A Review, *Industrial & Engineering Chemistry Research*, 2013, **52**, 3581-3599.
- 915 123. Z. Shayegan, F. Haghighat and C. S. Lee, Carbon-doped TiO<sub>2</sub> film to enhance visible and UV light  
916 photocatalytic degradation of indoor environment volatile organic compounds, *J. Environ.  
917 Chem. Eng.*, 2020, **8**, 14.
- 918 124. H.-H. Chun and W.-K. Jo, Adsorption and photocatalysis of 2-ethyl-1-hexanol over graphene  
919 oxide-TiO<sub>2</sub> hybrids post-treated under various thermal conditions, *Applied Catalysis B-  
920 Environmental*, 2016, **180**, 740-750.
- 921 125. E. Q. Yu, J. Chen and H. P. Jia, Enhanced light-driven photothermocatalytic activity on selectively  
922 dissolved LaTi<sub>1-x</sub>Mn<sub>x</sub>O<sub>3</sub>+delta perovskites by photoactivation, *Journal of Hazardous Materials*,  
923 2020, **399**, 11.
- 924 126. Y. Zhang, Y. X. Liu, S. H. Xie, H. B. Huang, G. S. Guo, H. X. Dai and J. G. Deng, Supported ceria-  
925 modified silver catalysts with high activity and stability for toluene removal, *Environ. Int.*, 2019,  
926 **128**, 335-342.
- 927 127. F. Montecchio, M. U. Babler and K. Engvall, Development of an irradiation and kinetic model  
928 for UV processes in volatile organic compounds abatement applications, *Chemical Engineering  
929 Journal*, 2018, **348**, 569-582.
- 930 128. M. J. Tian, F. Liao, Q. F. Ke, Y. J. Guo and Y. P. Guo, Synergetic effect of titanium dioxide ultralong  
931 nanofibers and activated carbon fibers on adsorption and photodegradation of toluene,  
932 *Chemical Engineering Journal*, 2017, **328**, 962-976.
- 933 129. X. Li, J. G. Yu, J. X. Low, Y. P. Fang, J. Xiao and X. B. Chen, Engineering heterogeneous  
934 semiconductors for solar water splitting, *J. Mater. Chem. A*, 2015, **3**, 2485-2534.
- 935 130. S. M. Fang, Y. Z. Li, Y. Yang, J. Chen, H. H. Liu and X. J. Zhao, Mg-doped OMS-2 nanorods: a highly  
936 efficient catalyst for purification of volatile organic compounds with full solar spectrum  
937 irradiation, *Environ. Sci.-Nano*, 2017, **4**, 1798-1807.
- 938 131. X. Li, J. Q. Wen, J. X. Low, Y. P. Fang and J. G. Yu, Design and fabrication of semiconductor  
939 photocatalyst for photocatalytic reduction of CO<sub>2</sub> to solar fuel, *Science China-Materials*, 2014,

- 940 **57**, 70-100.
- 941 132. F. Zhang, Y. Zhu, Q. Lin, L. Zhang, X. Zhang and H. Wang, Noble-metal single-atoms in  
942 thermocatalysis, electrocatalysis, and photocatalysis, *Energy & Environmental Science*, 2021,  
943 **14**, 2954-3009.
- 944 133. C. H. Nguyen, C. C. Fu and R. S. Juang, Degradation of methylene blue and methyl orange by  
945 palladium-doped TiO<sub>2</sub> photocatalysis for water reuse: Efficiency and degradation pathways, *J.*  
946 *Clean Prod.*, 2018, **202**, 413-427.
- 947 134. P. Garcia-Ramirez, E. Ramirez-Morales, J. C. S. Cortazar, I. Sires and S. Silva-Martinez, Influence  
948 of ruthenium doping on UV- and visible-light photoelectrocatalytic color removal from dye  
949 solutions using a TiO<sub>2</sub> nanotube array photoanode, *Chemosphere*, 2021, **267**, 10.
- 950 135. M. Perez-Gonzalez and S. A. Tomas, Surface chemistry of TiO<sub>2</sub>-ZnO thin films doped with Ag.  
951 Its role on the photocatalytic degradation of methylene blue, *Catalysis Today*, 2021, **360**, 129-  
952 137.
- 953 136. A. P. Manuel and K. Shankar, Hot Electrons in TiO<sub>2</sub>-Noble Metal Nano-Heterojunctions:  
954 Fundamental Science and Applications in Photocatalysis, *Nanomaterials*, 2021, **11**, 55.
- 955 137. S. I. Mogal, V. G. Gandhi, M. Mishra, S. Tripathi, T. Shripathi, P. A. Joshi and D. O. Shah, Single-  
956 Step Synthesis of Silver-Doped Titanium Dioxide: Influence of Silver on Structural, Textural, and  
957 Photocatalytic Properties, *Industrial & Engineering Chemistry Research*, 2014, **53**, 5749-5758.
- 958 138. X. C. Meng, H. N. Qin and Z. S. Zhang, New insight into the enhanced visible light-driven  
959 photocatalytic activity of Pd/PdCl<sub>2</sub>-doped Bi<sub>2</sub>WO<sub>6</sub> photocatalysts, *Journal of Colloid and*  
960 *Interface Science*, 2018, **513**, 877-890.
- 961 139. X. L. Xue, X. Y. Chen and X. W. Gong, Fast electron transfer and enhanced visible light  
962 photocatalytic activity of silver and Ag<sub>2</sub>O co-doped titanium dioxide with the doping of  
963 electron mediator for removing gaseous toluene, *Materials Science in Semiconductor*  
964 *Processing*, 2021, **132**.
- 965 140. C. V. Reddy, I. N. Reddy, B. Akkinapally, V. V. N. Harish, K. R. Reddy and S. Jaesool, Mn-doped  
966 ZrO<sub>2</sub> nanoparticles prepared by a template-free method for electrochemical energy storage  
967 and abatement of dye degradation, *Ceram. Int.*, 2019, **45**, 15298-15306.
- 968 141. T. Tsuzuki, R. L. He, A. Dodd and M. Saunders, Challenges in Determining the Location of  
969 Dopants, to Study the Influence of Metal Doping on the Photocatalytic Activities of ZnO  
970 Nanopowders, *Nanomaterials*, 2019, **9**.
- 971 142. X. Wang, M. Hong, F. Zhang, Z. Zhuang and Y. Yu, Recyclable Nanoscale Zero Valent Iron Doped  
972 g-C<sub>3</sub>N<sub>4</sub>/MoS<sub>2</sub> for Efficient Photocatalysis of RhB and Cr(VI) Driven by Visible Light, *ACS*  
973 *Sustainable Chemistry & Engineering*, 2016, **4**, 4055-4062.
- 974 143. P. K. Boruah, B. Sharma, I. Karbhal, M. V. Shelke and M. R. Das, Ammonia-modified graphene  
975 sheets decorated with magnetic Fe<sub>3</sub>O<sub>4</sub> nanoparticles for the photocatalytic and photo-Fenton  
976 degradation of phenolic compounds under sunlight irradiation, *Journal of Hazardous Materials*,  
977 2017, **325**, 90-100.
- 978 144. H. R. Rajabi, O. Khani, M. Shamsipur and V. Vatanpour, High-performance pure and Fe<sup>3+</sup>-ion  
979 doped ZnS quantum dots as green nanophotocatalysts for the removal of malachite green  
980 under UV-light irradiation, *Journal of Hazardous Materials*, 2013, **250**, 370-378.
- 981 145. J. N. Qu, Y. Du, P. H. Ji, Z. F. Li, N. Jiang, X. Y. Sun, L. Xue, H. Y. Li and G. L. Sun, Fe, Cu co-doped  
982 BiOBr with improved photocatalytic ability of pollutants degradation, *J. Alloy. Compd.*, 2021,  
983 **881**, 10.
- 984 146. H. Bantawal, U. S. Shenoy and D. K. Bhat, Vanadium-Doped SrTiO<sub>3</sub> Nanocubes: Insight into role  
985 of vanadium in improving the photocatalytic activity, *Appl. Surf. Sci.*, 2020, **513**, 7.
- 986 147. T. Wang, X. Q. Liu, D. L. Han, C. C. Ma, M. B. Wei, P. W. Huo and Y. S. Yan, Biomass derived the  
987 V-doped carbon/Bi<sub>2</sub>O<sub>3</sub> composite for efficient photocatalysts, *Environ. Res.*, 2020, **182**, 9.
- 988 148. I. N. Reddy, C. V. Reddy, J. Shim, B. Akkinapally, M. Y. Cho, K. Yoo and D. Kim, Excellent visible-  
989 light driven photocatalyst of (Al, Ni) co-doped ZnO structures for organic dye degradation,  
990 *Catalysis Today*, 2020, **340**, 277-285.
- 991 149. M. Afif, U. Sulaeman, A. Riapanitra, R. Andreas and S. Yin, Use of Mn doping to suppress defect  
992 sites in Ag<sub>3</sub>PO<sub>4</sub>: Applications in photocatalysis, *Appl. Surf. Sci.*, 2019, **466**, 352-357.
- 993 150. P. Herr, C. Kerzig, C. B. Larsen, D. Haussinger and O. S. Wenger, Manganese(i) complexes with  
994 metal-to-ligand charge transfer luminescence and photoreactivity, *Nat. Chem.*, DOI:  
995 10.1038/s41557-021-00744-9, 8.
- 996 151. P. Devaraji, N. K. Sathu and C. S. Gopinath, Ambient Oxidation of Benzene to Phenol by

- 997 Photocatalysis on Au/TiO<sub>2</sub>: Role of Holes, *Acs Catalysis*, 2014, **4**, 2844-2853.
- 998 152. M. Stucchi, D. C. Boffito, E. Pargoletti, G. Cerrato, C. L. Bianchi and G. Cappelletti, Nano-MnO<sub>2</sub>  
999 Decoration of TiO<sub>2</sub> Microparticles to Promote Gaseous Ethanol Visible Photoremoval,  
1000 *Nanomaterials*, 2018, **8**.
- 1001 153. R. C. Li, B. H. Hu, T. W. Yu, Z. P. Shao, Y. Wang and S. Q. Song, New TiO<sub>2</sub>-Based Oxide for  
1002 Catalyzing Alkaline Hydrogen Evolution Reaction with Noble Metal-Like Performance, *Small*  
1003 *Methods*, 2021, **5**, 9.
- 1004 154. S. Shamaila, T. Bano and A. K. L. Sajjad, Efficient visible light magnetic modified iron oxide  
1005 photocatalysts, *Ceram. Int.*, 2017, **43**, 14672-14677.
- 1006 155. J. R. Xiao, T. Y. Peng, R. Li, Z. H. Peng and C. H. Yan, Preparation, phase transformation and  
1007 photocatalytic activities of cerium-doped mesoporous titania nanoparticles, *Journal of Solid*  
1008 *State Chemistry*, 2006, **179**, 1161-1170.
- 1009 156. H. G. Wang, F. F. Wen, X. Y. Li, X. R. Gan, Y. N. Yang, P. Chen and Y. Zhang, Cerium-doped MoS<sub>2</sub>  
1010 nanostructures: Efficient visible photocatalysis for Cr(VI) removal, *Sep. Purif. Technol.*, 2016,  
1011 **170**, 190-198.
- 1012 157. H. Gandelman, A. L. da Silva, B. Ramos and D. Gouvea, Interface excess on Sb-doped TiO<sub>2</sub>  
1013 photocatalysts and its influence on photocatalytic activity, *Ceram. Int.*, 2021, **47**, 619-625.
- 1014 158. O. Aviles-Garcia, J. Espino-Valencia, R. Romero, J. L. Rico-Cerda, M. Arroyo-Albiter and R.  
1015 Natividad, W and Mo doped TiO<sub>2</sub>: Synthesis, characterization and photocatalytic activity, *Fuel*,  
1016 2017, **198**, 31-41.
- 1017 159. K. Goswami and R. Ananthkrishnan, Ce-Doped CuMgAl Oxide as a Redox Couple Mediated  
1018 Catalyst for Visible Light Aided Photooxidation of Organic Pollutants, *Acs Applied Nano*  
1019 *Materials*, 2019, **2**, 6030-6039.
- 1020 160. Z. Shayegan, F. Haghightat and C. S. Lee, Surface fluorinated Ce-doped TiO<sub>2</sub> nanostructure  
1021 photocatalyst: A trap and remove strategy to enhance the VOC removal from indoor air  
1022 environment, *Chemical Engineering Journal*, 2020, **401**.
- 1023 161. X. F. Peng, C. H. Wang, Y. Y. Li, H. Ma, F. Yu, G. S. Che, J. Y. Yan, X. T. Zhang and Y. C. Liu, Revisiting  
1024 cocatalyst/TiO<sub>2</sub> photocatalyst in blue light photothermal catalysis, *Catalysis Today*, 2019, **335**,  
1025 286-293.
- 1026 162. Y. Huang, Z. Guo, H. Liu, S. Zhang, P. Wang, J. Lu and Y. Tong, Heterojunction Architecture of N-  
1027 Doped WO<sub>3</sub> Nanobundles with Ce<sub>2</sub>S<sub>3</sub> Nanodots Hybridized on a Carbon Textile Enables a  
1028 Highly Efficient Flexible Photocatalyst, *Advanced Functional Materials*, 2019, **29**.
- 1029 163. H. Che, G. Che, P. Zhou, C. Liu, H. Dong, C. Li, N. Song and C. Li, Nitrogen doped carbon ribbons  
1030 modified g-C<sub>3</sub>N<sub>4</sub> for markedly enhanced photocatalytic H<sub>2</sub>-production in visible to near-  
1031 infrared region, *Chemical Engineering Journal*, 2020, **382**.
- 1032 164. S. Wu, H. Hu, Y. Lin, J. Zhang and Y. H. Hu, Visible light photocatalytic degradation of tetracycline  
1033 over TiO<sub>2</sub>, *Chemical Engineering Journal*, 2020, **382**.
- 1034 165. G. S. Jamila, S. Sajjad, S. A. K. Leghari and M. Long, Nitrogen doped carbon quantum dots and  
1035 GO modified WO<sub>3</sub> nanosheets combination as an effective visible photo catalyst, *Journal of*  
1036 *Hazardous Materials*, 2020, **382**.
- 1037 166. G. S. Jamila, S. Sajjad, S. A. K. Leghari and T. Mahmood, Role of nitrogen doped carbon quantum  
1038 dots on CuO nano-leaves as solar induced photo catalyst, *Journal of Physics and Chemistry of*  
1039 *Solids*, 2020, **138**.
- 1040 167. J. Lu, Y. Wang, J. Huang, J. Fei, L. Cao and C. Li, In situ synthesis of mesoporous C-doped TiO<sub>2</sub>  
1041 single crystal with oxygen vacancy and its enhanced sunlight photocatalytic properties, *Dyes*  
1042 *and Pigments*, 2017, **144**, 203-211.
- 1043 168. J. Matos, J. Ocares-Riquelme, P. S. Poon, R. Montana, X. Garcia, K. Campos, J. C. Hernandez-  
1044 Garrido and M. M. Titirici, C-doped anatase TiO<sub>2</sub>: Adsorption kinetics and photocatalytic  
1045 degradation of methylene blue and phenol, and correlations with DFT estimations, *Journal of*  
1046 *Colloid and Interface Science*, 2019, **547**, 14-29.
- 1047 169. S. Wang, X. Zhang, S. Li, Y. Fang, L. Pan and J.-J. Zou, C-doped ZnO ball-in-ball hollow  
1048 microspheres for efficient photocatalytic and photoelectrochemical applications, *Journal of*  
1049 *Hazardous Materials*, 2017, **331**, 235-245.
- 1050 170. Z. Ma, Y. Li, Y. Lv, R. Sa, Q. Li and K. Wu, Synergistic Effect of Doping and Compositing on  
1051 Photocatalytic Efficiency: A Case Study of La<sub>2</sub>Ti<sub>2</sub>O<sub>7</sub>, *ACS Appl. Mater. Interfaces*, 2018, **10**,  
1052 39327-39335.
- 1053 171. C. Feng, L. Tang, Y. Deng, G. Zeng, J. Wang, Y. Liu, Z. Chen, J. Yu and J. Wang, Enhancing optical

- 1054 absorption and charge transfer: Synthesis of S-doped h-BN with tunable band structures for  
1055 metal-free visible-light-driven photocatalysis, *Applied Catalysis B-Environmental*, 2019, **256**.
- 1056 172. M. A. Baghchesara, H. R. Azimi, A. G. Shiravizadeh, M. A. M. Teridi and R. Yousefi, Improving  
1057 the intrinsic properties of rGO sheets by S-doping and the effects of rGO improvements on the  
1058 photocatalytic performance of Cu<sub>3</sub>Se<sub>2</sub>/rGO nanocomposites, *Appl. Surf. Sci.*, 2019, **466**, 401-  
1059 410.
- 1060 173. R. Wang, D. Li, H. Wang, C. Liu and L. Xu, Preparation, Characterization, and Performance  
1061 Analysis of S-Doped Bi<sub>2</sub>MoO<sub>6</sub> Nanosheets, *Nanomaterials*, 2019, **9**.
- 1062 174. Y. Shi, G. Zhan, H. Li, X. Wang, X. Liu, L. Shi, K. Wei, C. Ling, Z. Li, H. Wang, C. Mao, X. Liu and L.  
1063 Zhang, Simultaneous Manipulation of Bulk Excitons and Surface Defects for Ultrastable and  
1064 Highly Selective CO<sub>2</sub> Photoreduction, *Adv. Mater.*, 2021, DOI: 10.1002/adma.202100143.
- 1065 175. Y. Dong, D. Xu, Q. Wang, G. Zhang, Q. Zhang, Z. Zhang, L. Lv, Y. Xia, Z. Ren and P. Wang, Tailoring  
1066 the electronic structure of ultrathin 2D Bi<sub>3</sub>O<sub>4</sub>Cl sheets by boron doping for enhanced visible  
1067 light environmental remediation, *Appl. Surf. Sci.*, 2021, **542**.
- 1068 176. Q. Wang, B. Rhimi, H. Wang and C. Y. Wang, Efficient photocatalytic degradation of gaseous  
1069 toluene over F-doped TiO<sub>2</sub>/exfoliated bentonite, *Appl. Surf. Sci.*, 2020, **530**, 12.
- 1070 177. A. Khalilzadeh and S. Fatemi, Spouted bed reactor for VOC removal by modified nano-TiO<sub>2</sub>  
1071 photocatalytic particles, *Chemical Engineering Research & Design*, 2016, **115**, 241-250.
- 1072 178. M. Kamaei, H. Rashedi, S. M. M. Dastgheib and S. Tasharrofi, Comparing Photocatalytic  
1073 Degradation of Gaseous Ethylbenzene Using N-doped and Pure TiO<sub>2</sub> Nano-Catalysts Coated on  
1074 Glass Beads under Both UV and Visible Light Irradiation, *Catalysts*, 2018, **8**.
- 1075 179. E. W. Awin, A. Lale, K. C. H. Kumar, S. Bernard and R. Kumar, Disordered mesoporous polymer  
1076 derived N-doped TiO<sub>2</sub>/Si-O-C-N nanocomposites with nanoscaled heterojunctions towards  
1077 enhanced adsorption and harnessing of visible light, *Appl. Surf. Sci.*, 2020, **508**.
- 1078 180. M. L. Sun, X. A. Dong, B. Lei, J. Y. Li, P. Chen, Y. X. Zhang and F. Dong, Graphene oxide mediated  
1079 co-generation of C-doping and oxygen defects in Bi<sub>2</sub>WO<sub>6</sub> nanosheets: a combined DRIFTS and  
1080 DFT investigation, *Nanoscale*, 2019, **11**, 20562-20570.
- 1081 181. W. Y. Diao, J. Y. Xu, X. Rao and Y. P. Zhang, Facile Synthesis of Fluorine Doped Rutile TiO<sub>2</sub>  
1082 Nanorod Arrays for Photocatalytic Removal of Formaldehyde, *Catalysis Letters*, DOI:  
1083 10.1007/s10562-021-03700-x.
- 1084 182. P. Ramacharyulu, J. P. Kumar, G. K. Prasad and B. Sreedhar, Sulphur doped nano TiO<sub>2</sub>: Synthesis,  
1085 characterization and photocatalytic degradation of a toxic chemical in presence of sunlight,  
1086 *Materials Chemistry and Physics*, 2014, **148**, 692-698.
- 1087 183. R. Asahi, T. Morikawa, H. Irie and T. Ohwaki, Nitrogen-Doped Titanium Dioxide as Visible-Light-  
1088 Sensitive Photocatalyst: Designs, Developments, and Prospects, *Chem. Rev.*, 2014, **114**, 9824-  
1089 9852.
- 1090 184. S. L. Yang, L. Peng, P. P. Huang, X. S. Wang, Y. B. Sun, C. Y. Cao and W. G. Song, Nitrogen,  
1091 Phosphorus, and Sulfur Co-Doped Hollow Carbon Shell as Superior Metal-Free Catalyst for  
1092 Selective Oxidation of Aromatic Alkanes, *Angew. Chem.-Int. Edit.*, 2016, **55**, 4016-4020.
- 1093 185. Y. Wu, H. Wang, W. Tu, Y. Liu, Y. Z. Tan, X. Z. Yuan and J. W. Chew, Quasi-polymeric construction  
1094 of stable perovskite-type LaFeO<sub>3</sub>/g-C<sub>3</sub>N<sub>4</sub> heterostructured photocatalyst for improved Z-  
1095 scheme photocatalytic activity via solid p-n heterojunction interfacial effect, *Journal of*  
1096 *Hazardous Materials*, 2018, **347**, 412-422.
- 1097 186. H. L. Liu, X. Y. Chang, X. X. Liu, G. Y. Li, W. P. Zhang and T. C. An, Boosting the photocatalytic  
1098 degradation of ethyl acetate by a Z-scheme Au-TiO<sub>2</sub>@NH<sub>2</sub>-UiO-66 heterojunction with  
1099 ultrafine Au as an electron mediator, *Environ. Sci.-Nano*, 2021, **8**, 2542-2553.
- 1100 187. A. Enesca and L. Isac, Photocatalytic Activity of Cu<sub>2</sub>S/WO<sub>3</sub> and Cu<sub>2</sub>S/SnO<sub>2</sub> Heterostructures  
1101 for Indoor Air Treatment, *Materials*, 2021, **14**.
- 1102 188. G. P. Dai, J. G. Yu and G. Liu, Synthesis and Enhanced Visible-Light Photoelectrocatalytic Activity  
1103 of p-n Junction BiOI/TiO<sub>2</sub> Nanotube Arrays, *Journal of Physical Chemistry C*, 2011, **115**, 7339-  
1104 7346.
- 1105 189. H. Guo, C. G. Niu, D. W. Huang, N. Tang, C. Liang, L. Zhang, X. J. Wen, Y. Yang, W. J. Wang and G.  
1106 M. Zeng, Integrating the plasmonic effect and p-n heterojunction into a novel  
1107 Ag/Ag<sub>2</sub>O/PbBiO<sub>2</sub>Br photocatalyst: Broadened light absorption and accelerated charge  
1108 separation co-mediated highly efficient visible/NIR light photocatalysis, *Chemical Engineering*  
1109 *Journal*, 2019, **360**, 349-363.
- 1110 190. H. W. Huang, K. Xiao, Y. He, T. R. Zhang, F. Dong, X. Du and Y. H. Zhang, In situ assembly of



1111 BiOI@Bi<sub>2</sub>O<sub>3</sub>/TiO<sub>2</sub> p-n junction: charge induced unique front-lateral surfaces coupling  
1112 heterostructure with high exposure of BiOI {001} active facets for robust and nonselective  
1113 photocatalysis, *Applied Catalysis B-Environmental*, 2016, **199**, 75-86.

1114 191. A. Iqbal, S. Sajjad and S. A. K. Leghari, Low Cost Graphene Oxide Modified Alumina  
1115 Nanocomposite as Solar Light Induced Photocatalyst, *Acs Applied Nano Materials*, 2018, **1**,  
1116 4612-4621.

1117 192. S. Sajjad, M. Khan, S. A. K. Leghari, N. A. Ryma and S. A. Farooqi, Potential visible WO<sub>3</sub>/GO  
1118 composite photocatalyst, *International Journal of Applied Ceramic Technology*, 2019, **16**, 1218-  
1119 1227.

1120 193. Z. Y. Yao, H. J. Sun, S. B. Xiao, Y. L. Hu, X. F. Liu and Y. Zhang, Synergetic piezo-photocatalytic  
1121 effect in a Bi<sub>2</sub>MoO<sub>6</sub>/BiOBr composite for decomposing organic pollutants, *Appl. Surf. Sci.*, 2021,  
1122 **560**.

1123 194. J. Q. Pan, C. Y. Chi, M. Z. You, Z. Y. Jiang, W. J. Zhao, M. Zhu, C. S. Song, Y. Y. Zheng and C. R. Li,  
1124 The three dimensional Z-scheme Ag<sub>3</sub>PO<sub>4</sub>/Ag/MoS<sub>2</sub>/TiO<sub>2</sub> nano-heterojunction and its sunlight  
1125 photocatalytic performance enhancement, *Materials Letters*, 2018, **227**, 205-208.

1126 195. X. G. Wang, M. H. Sun, M. Murugananthan, Y. R. Zhang and L. Z. Zhang, Electrochemically self-  
1127 doped WO<sub>3</sub>/TiO<sub>2</sub> nanotubes for photocatalytic degradation of volatile organic compounds,  
1128 *Applied Catalysis B-Environmental*, 2020, **260**, 11.

1129 196. M. M. Ding, W. Ao, H. Xu, W. Chen, L. Tao, Z. Shen, H. H. Liu, C. H. Lu and Z. L. Xie, Facile  
1130 construction of dual heterojunction CoO@TiO<sub>2</sub>/MXene hybrid with efficient and stable  
1131 catalytic activity for phenol degradation with peroxymonosulfate under visible light irradiation,  
1132 *Journal of Hazardous Materials*, 2021, **420**.

1133 197. W. J. Wang, W. Q. Gu, G. Y. Li, H. J. Xie, P. K. Wong and T. C. An, Few-layered tungsten selenide  
1134 as a co-catalyst for visible-light-driven photocatalytic production of hydrogen peroxide for  
1135 bacterial inactivation, *Environ. Sci.-Nano*, 2020, **7**, 3877-3887.

1136 198. J. Shen, R. Wang, Q. Q. Liu, X. F. Yang, H. Tang and J. Yang, Accelerating photocatalytic hydrogen  
1137 evolution and pollutant degradation by coupling organic co-catalysts with TiO<sub>2</sub>, *Chinese Journal*  
1138 *of Catalysis*, 2019, **40**, 380-389.

1139 199. S. Bai, L. M. Wang, X. Y. Chen, J. T. Du and Y. J. Xiong, Chemically exfoliated metallic MoS<sub>2</sub>  
1140 nanosheets: A promising supporting co-catalyst for enhancing the photocatalytic performance  
1141 of TiO<sub>2</sub> nanocrystals, *Nano Res.*, 2015, **8**, 175-183.

1142 200. L. Q. Ye, Y. R. Su, X. L. Jin, H. Q. Xie and C. Zhang, Recent advances in BiOX (X = Cl, Br and I)  
1143 photocatalysts: synthesis, modification, facet effects and mechanisms, *Environ. Sci.-Nano*, 2014,  
1144 **1**, 90-112.

1145 201. Y. Liang, Y. Yang, C. W. Zou, K. Xu, X. F. Luo, T. Luo, J. Y. Li, Q. Yang, P. Y. Shi and C. L. Yuan, 2D  
1146 ultra-thin WO<sub>3</sub> nanosheets with dominant {002} crystal facets for high-performance xylene  
1147 sensing and methyl orange photocatalytic degradation, *J. Alloy. Compd.*, 2019, **783**, 848-854.

1148 202. J. C. C. Yu, V. H. Nguyen, J. Lasek and J. C. S. Wu, Titania nanosheet photocatalysts with  
1149 dominantly exposed (001) reactive facets for photocatalytic NO<sub>x</sub> abatement, *Applied Catalysis*  
1150 *B-Environmental*, 2017, **219**, 391-400.

1151 203. H. Li, F. Deng, Y. Zheng, L. Hua, C. H. Qu and X. B. Luo, Visible-light-driven Z-scheme rGO/Bi<sub>2</sub>S<sub>3</sub>-  
1152 BiOBr heterojunctions with tunable exposed BiOBr (102) facets for efficient synchronous  
1153 photocatalytic degradation of 2-nitrophenol and Cr(vi) reduction, *Environ. Sci.-Nano*, 2019, **6**,  
1154 3670-3683.

1155